# Geological carbon cycle constraints on the terrestrial hydrological response to higher atmospheric $CO_2$

Jeremy Kesner Caves Rugenstein[1] and Alexander J Winkler[2]

[1]Colorado State University
[2]Max Planck Institute for Meteorology

January 20, 2023

## Abstract

How runoff will change as atmospheric $CO_2$ rises depends upon several difficult to project factors, including $CO_2$ fertilization, lengthened growing seasons, and vegetation greening. However, geologic records of the hydrological response to past carbon cycle perturbations indicate large increases in runoff with higher $CO_2$. We demonstrate that the fact that the Earth has remained habitable since life emerged sets a lower-bound on the sensitivity of runoff to $CO_2$ changes. The recovery of the Earth system from perturbations is attributed to silicate weathering, which transfers $CO_2$ to the oceans as alkalinity via runoff. Though many factors mediate weathering rates, runoff determines the total flux of silicate-derived cations and hence the removal flux of excess $CO_2$. Using a carbon cycle model that parameterizes weathering as a function of rock reactivity, runoff, temperature, and soil $CO_2$, we show that recovery from a perturbation is only possible if the lower-bound for the sensitivity of runoff to atmospheric $CO_2$ is 0%/K. Using proxy data for the Paleocene-Eocene Thermal Maximum, we find that to match the marine $d^{13}C$ record requires a runoff sensitivity greater than 0%/K and similar to estimates of the modern runoff sensitivity derived from an ensemble of Earth system models. These results suggest that the processes that enhance global runoff are likely to prevail over processes that tend to dampen runoff. In turn, that the Earth has always recovered from perturbations suggests that, though the runoff response is spatially complex, global discharge has never declined in response to warming, despite quite varied paleogeographies.

# GEOLOGIC CARBON CYCLE CONSTRAINTS ON THE TERRESTRIAL HYDROLOGICAL RESPONSE TO HIGHER ATMOSPHERIC $CO_2$

Jeremy K. Caves Rugenstein[1,2] and Alexander J. Winkler[2,3]

[1]Department of Geosciences, Colorado State University, Fort Collins, CO, USA
[2]Max Planck Institute for Meteorology, Hamburg, Germany
[3]Max Planck Institute for Biogeochemistry, Jena, Germany

**Key Points**:
1. The silicate weathering negative feedback depends upon runoff to drive recovery from carbon cycle perturbations.
2. Decreases in runoff with warming would lead to runaway greenhouse states.
3. The sensitivity of runoff to warming has a lower-bound of 0%/K as dictated by carbon cycle constraints.

**Abstract**

How runoff will change as atmospheric $CO_2$ rises depends upon several difficult to project factors, including $CO_2$ fertilization, lengthened growing seasons, and vegetation greening. However, geologic records of the hydrological response to past carbon cycle perturbations indicate large increases in runoff with higher $CO_2$. We demonstrate that the fact that the Earth has remained habitable since life emerged sets a lower-bound on the sensitivity of runoff to $CO_2$ changes. The recovery of the Earth system from perturbations is attributed to silicate weathering, which transfers $CO_2$ to the oceans as alkalinity via runoff. Though many factors mediate weathering rates, runoff determines the total flux of silicate-derived cations and hence the removal flux of excess $CO_2$. Using a carbon cycle model that parameterizes weathering as a function of rock reactivity, runoff, temperature, and soil $CO_2$, we show that recovery from a perturbation is only possible if the lower-bound for the sensitivity of runoff to atmospheric $CO_2$ is 0%/K. Using proxy data for the Paleocene-Eocene Thermal Maximum, we find that to match the marine $\delta^{13}C$ record requires a runoff sensitivity greater than 0%/K and similar to estimates of the modern runoff sensitivity derived from an ensemble of Earth system models. These results suggest that the processes that enhance global runoff are likely to prevail over processes that tend to dampen runoff. In turn, that the Earth has always recovered from perturbations suggests that, though the runoff response is spatially complex, global discharge has never declined in response to warming, despite quite varied paleogeographies.

**Plain Language Summary**

Runoff—the quantity of water delivered by rivers to the ocean—is likely to change as the climate warms. However, because generation of runoff involves many small-scale processes, it is difficult to forecast how global patterns of runoff will change as atmospheric $CO_2$ rises. We take advantage of the fact that runoff is the primary mechanism that transfers excess $CO_2$ from the atmosphere to the ocean for eventual burial as carbonate rock. It is this process that permits the Earth to recover from major perturbations. We find that runoff must increase in a warmer world; if it did not, then atmospheric $CO_2$ would continually increase in the atmosphere, leading to a runaway greenhouse. This hard constraint places a lower-bound on how runoff must change in response to rising atmospheric $CO_2$.

## 1. Introduction

Runoff—the transfer of water from the continents to the oceans and to closed basins— is a critical component of the Earth system. Runoff ($q$) determines the amount of freshwater available for societal use, transports nutrients from upland landscapes to lowland and marine ecosystems and provides the water necessary to weather rocks that sequester atmospheric $CO_2$. Despite its importance for the functioning of the Earth system and for societies, how $q$ will change as atmospheric $CO_2$ rises remains highly uncertain. Part of this uncertainty arises because the hydrological cycle is comprised of a number of different and interacting components—including precipitation ($P$), bare-soil and vegetation-controlled evaporation ($ET$), and $q$—which may respond differently to rising atmospheric $CO_2$ and temperature (Milly & Dunne, 2016). For some components, there are well grounded theoretical expectations for how they should change. Precipitation globally is thought to increase by approximately 2%/K given constraints on how much energy is available for evaporation (Held & Soden, 2006; Pendergrass & Hartmann, 2014). Potential evapotranspiration ($PET$) over land should also increase, as rising temperatures drive increases in the saturation vapor deficit. This increase in $PET$ is robustly predicted to be larger than the increase in $P$ (Scheff & Frierson, 2014).

Collectively, these expectations—combined with observations that support them— suggest that much of the land surface will become more arid with warming (Cook et al., 2014; Ficklin & Novick, 2017; Mankin et al., 2019; Milly & Dunne, 2020; Novick et al., 2016; Overpeck & Udall, 2020). However, there remain two critical, linked components of the hydrological cycle for which theoretical expectations and observational constraints are of low-confidence and poor—actual $ET$ and $q$ (Douville et al., 2021). $ET$ determines how much $P$ is returned to the atmosphere and how much is partitioned to $q$; as a consequence, $ET$ and $P$ determine surface water availability. Vegetation water use (*i.e.*, transpiration) is thought to be the predominant component of $ET$ (~ 60%) (Good et al., 2015; Schlesinger & Jasechko, 2014; Wei et al., 2017); vegetation additionally impacts another 10-15% of $ET$ due to intercepted $P$ that evaporates directly from the leaf or woody surface (Wang-Erlandsson et al., 2014). Thus, in addition to the physical response to $CO_2$ increase ($P$ and $PET$), the global vegetation response to rising $CO_2$ will further determine the trajectory of surface water availability.

However, projecting how global vegetation will change and its impact on $q$ remains difficult. Though leaf-level transpiration is expected to decrease as $CO_2$ rises, total leaf area is expected to increase; the competition of these two processes globally will partially determine the total change in $q$. Satellite observations indicate that the world is overwhelmingly greening and that this greening is leading to greater $ET$ (Forzieri et al., 2020; Winkler et al., 2021; Zhu

88   et al., 2016). In semi-arid regions, observations indicate this greening and associated increase

89   in $ET$ has led to declining $q$ (Ukkola et al., 2016), and many land-surface models—which are

90   designed to encapsulate a number of specific plant physiological process—find that increases

91   in leaf area have been substantial enough to reduce $q$ globally (Forzieri et al., 2020; Piao et al.,

92   2007). In contrast, coupled land-atmosphere models find that, while the Earth's surface greens

93   substantially, the resulting increase in $ET$ fluxes is less than the increase in $P$ (Lemordant et

94   al., 2018; Swann et al., 2016). Though this prediction is spatially heterogeneous (Mankin et al.,

95   2019) and of low-confidence, the mean global average change in $q$ with temperature is

96   predicted to be ~2.9 ± 1 %/K across the CMIP5 ensemble using the RCP8.5 scenario (Zhang

97   et al., 2014). Much of this increase is driven by widespread model agreement of increasing $q$

98   in the northern high latitudes (Scheff et al., 2017). However, there remain serious questions

99   about how leaf-level processes and slower vegetation responses (*i.e.*, species compositional

100  changes) are parameterized within these coupled models. As a consequence, there is no firm

101  theoretical expectation nor well-constrained observations to indicate whether global $ET$ will

102  increase or decrease relative to $P$ and, therefore, how globally averaged $q$ will change as

103  atmospheric $CO_2$ rises.

104      This disagreement and uncertainty regarding the direction and magnitude of the global

105  $q$ change as $CO_2$ rises stands in sharp contrast to both geologic observations of the hydrological

106  response to increasing $CO_2$ and theory regarding how the Earth system has recovered from

107  large carbon cycle perturbations in the geologic past. These recoveries are mediated by the

108  weathering of silicate rocks, which converts atmospheric $CO_2$ to alkalinity and permanently

109  buries carbon in marine sediments (R. A. Berner & Kothavala, 2001; Penman et al., 2020).

110  Critically, the weathering of rocks and transport of alkalinity to the ocean is thought to be

111  mediated primarily by $q$ (Kump et al., 2000; Li et al., 2022; Maher & Chamberlain, 2014; Otto-

112  Bliesner, 1995; Park et al., 2020), both to supply water to the weathering zone and to transport

113  the products of weathering to the ocean. The fact that life has persisted on Earth for more than

114  3 Ga indicates that this feedback must be particularly robust, capable of regulating Earth's

115  climate largely independent of the precise position of the continents, extant flora and fauna,

116  and magnitude and nature of the various climatic perturbations that have befallen Earth over

117  its history (Sagan & Mullen, 1972; Walker et al., 1981). Similarly, a growing body of literature

118  suggests that these past perturbations caused dramatic reorganizations of the terrestrial

119  hydrological cycle, recorded as thick packages of coarse-grained fluvial sediments during peak

120  warming (Chen et al., 2018; Foreman et al., 2012) and enhanced fluxes of nutrients and silica

121 to the ocean as reflected in widespread marine anoxia and chert deposits during many of these
122 carbon cycle perturbations (Penman, 2016; Them et al., 2017).

123     Here, we exploit this fundamental negative feedback in the Earth system and its
124 relationship with $q$ to provide a lower bound on how globally $q$ must respond to changes in
125 atmospheric $CO_2$. To constrain how $q$ must respond to changes in atmospheric $CO_2$, we employ
126 a version of a geological carbon cycle model that has been modified to represent the explicit
127 role of $q$ in modulating weathered solute concentrations and fluxes. We demonstrate that the
128 operation of this weathering feedback requires that $q$ does not decrease with rising atmospheric
129 $CO_2$ and, most likely, is positively sensitive to changes in $CO_2$, such that the flux of weathered
130 material always increases if $CO_2$ rapidly increases in the atmosphere. We further test this model
131 against geological data from the Paleocene-Eocene Thermal Maximum (PETM), and
132 demonstrate that, to match geological proxy data from the PETM requires that globally
133 averaged $q$ increase with atmospheric $CO_2$. We conclude by discussing how these constraints
134 on the sensitivity of the hydrological cycle carries profound implications for our understanding
135 of biogeochemical cycles in Earth's past and for Earth's future as $CO_2$ rises.

136

137     **2.  Background**

138     *2.1 Silicate Weathering and Runoff*

139     Silicate weathering is thought to be the primary process that removes $CO_2$ from the
140 coupled atmosphere-ocean system on geological timescales, neutralizing the input of $CO_2$ from
141 volcanoes (R. A. Berner & Kothavala, 2001). Silicate weathering is also thought to be sensitive
142 to climate, such that increases in the input flux of $CO_2$ and the resulting rise in atmospheric
143 $CO_2$ causes increased silicate weathering fluxes, which removes this excess $CO_2$ from the
144 Earth's surface (Robert A. Berner & Caldeira, 1997; Zeebe & Caldeira, 2008). Though other
145 Earth surface processes are important for the geological carbon cycle, including the weathering
146 and burial of organic carbon and oxidation/reduction of sulfur (Hilton & West, 2020; Torres et
147 al., 2014), the evidence for these processes being sensitive to climate—and therefore capable
148 of providing a negative feedback on atmospheric $CO_2$—is less extensive. Further, the reaction
149 of silicate rocks with $CO_2$ dissolved in water (*i.e.*, carbonic acid) is likely to have been
150 applicable for the entirety of Earth history. Critically, both data and models suggest that Earth
151 system recovery once a perturbation ceases typically occurs within 1 Myr or less (Bowen,
152 2013; Colbourn et al., 2015; Lenton & Britton, 2006; Uchikawa & Zeebe, 2008).

153        Equation 1 describes the long-term relationship between total carbon in the ocean-

154    atmosphere system ($M$; mol C) and the input and output fluxes of $CO_2$ (Caves et al., 2016;

155    Kump & Arthur, 1999):

156

157    $\frac{dM}{dt} = I - F_{silw}$            (Eq. 1)

158

159    where $F_{silw}$ is the silicate weathering flux [mol C/yr] and $I$ is the sum of the primary remaining

160    input and output fluxes of $CO_2$ [mol C/yr], including $CO_2$ from volcanism and solid Earth

161    degassing and organic carbon weathering and burial. On timescales longer than ocean

162    overturning, changes in the atmospheric partial pressure of $CO_2$ ($pCO_2$) are proportional to

163    changes in $M$. The global silicate weathering flux is defined as (White & Blum, 1995):

164

165    $F_{silw} = Q \times [C]_{sil}$            (Eq. 2)

166

167    where $Q$ is global discharge [L/yr] and $[C]_{sil}$ is the global average concentration of bicarbonate

168    ($HCO_3^-$) derived from the weathering of silicate rocks [mol C/L]. $Q$ is related to $q$ via the global

169    land area [$m^2$] ($Q = q \times area$), which, for the purposes of our simulations, we assume to be

170    constant. Consequently, for silicate weathering to act as a negative feedback on atmospheric

171    $CO_2$, either $q$, $[C]_{sil}$, or both must be sensitive to climate.

172        To demonstrate this, we use CH2O-CHOO (the Carbon-$H_2O$ Coupled HydrOlOgical

173    model), a modified version of CLiBeSO-W, which is a geological carbon cycle model that

174    calculates the mass balance of carbon and alkalinity in the ocean-atmosphere system (Caves

175    Rugenstein et al., 2019), and uses equation 2 to calculate $F_{silw}$. We first treat $q$ and $[C]_{sil}$ as

176    being independently sensitivity to $CO_2$-induced global warming (*i.e.*, $\Delta q$ and $\Delta[C]_{sil}$ have units

177    of %/K) and assume a climate sensitivity of 4K/$CO_2$ doubling (Knutti et al., 2017). In these

178    simulations, we inject 1000 Pg C into the atmosphere over 100 years and calculate the amount

179    of time required for atmospheric $CO_2$ to return to its initial value—termed the recovery time

180    [yr].

181        As shown in Figure 1, a negative sensitivity in either $q$ or $[C]_{sil}$ with temperature

182    requires a correspondingly larger sensitivity in the other parameter. Recovery from

183    perturbations is fastest when both parameters have a positive sensitivity, but small, positive

184    sensitivities still result in recovery times greater than 1 Ma. Thus, to place constraints on the

185    sensitivity of $q$ to $CO_2$ requires knowledge of how $[C]_{sil}$ will respond to atmospheric $CO_2$.

186    Recent advances in biogeochemistry, however, have resulted in improved constraints on how

187    $[C]_{sil}$ is likely to change with climate (Godsey et al., 2009, 2019; Li et al., 2022; Maher &

188    Chamberlain, 2014; West, 2012; Winnick & Maher, 2018). Following previous work, we

189    consider here three parameters that are likely to have the greatest impact on $[C]_{sil}$ and which

190    are also sensitive to climate: temperature ($T$), runoff ($q$), and soil $pCO_2$.
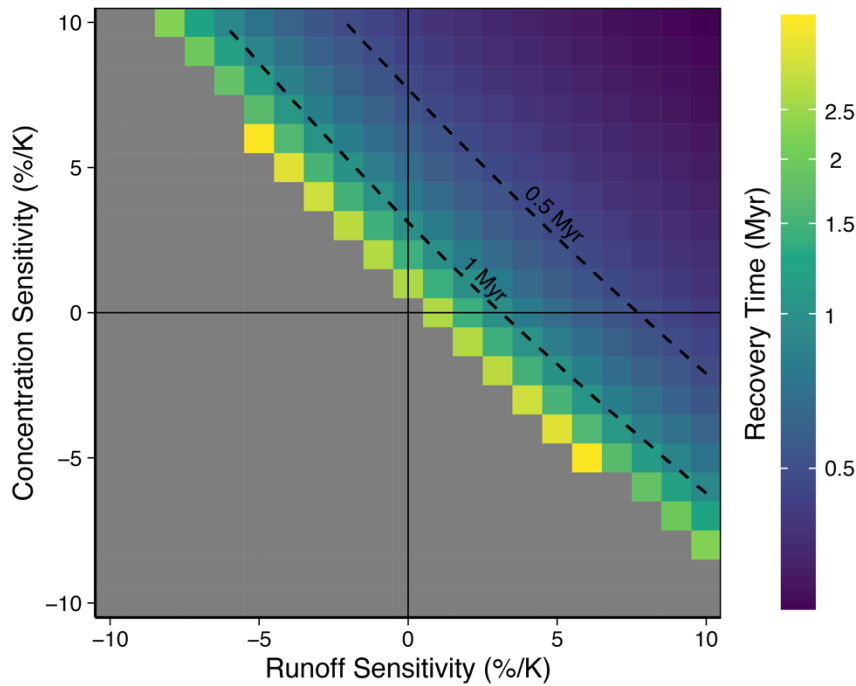


191

*Figure 1*: The time required for atmospheric $CO_2$ to recover to pre-perturbation values (shading

in $10^6$ yr) as a function of the $q$-sensitivity (%/K) and $[C]_{sil}$-sensitivity (%/K). Gray shading

indicates that atmospheric $CO_2$ does not return to pre-perturbation values within 4 Ma post-

perturbation. Solid lines denote the 0% $q$- and $[C]_{sil}$-sensitivities; dashed lines denote the 0.5

and 1 Myr recovery time contours.

197

198    To encapsulate these three terms, we use a recently developed reactive-transport model

199    of solute generation from Maher and Chamberlain (2014) to predict $[C]_{sil}$ (also termed the

200    MAC model (Baum et al., 2022; Graham & Pierrehumbert, 2020). Critically, this model also

201    permits us to explicitly treat the reactivity of the land surface—set by erosion and by the type

202    of exposed lithologies on Earth's surface (Caves Rugenstein et al., 2019; Ibarra et al., 2016;

203    West, 2012)—and which determines the rate at which silicate weathering occurs. These

204    equations are summarized in the Supporting Information, but are briefly described here.

205    Temperature affects $[C]_{sil}$ through its impact on net reaction rates, as parameterized by an

206    Arrhenius equation. Runoff affects $[C]_{sil}$ via dilution, though only in weathering systems that

207    are kinetically limited; whether $[C]_{sil}$ is kinetically-limited depends upon the reactivity of the

208    weathering material, which is parameterized as a function of the age of the weathering zone
209    ($Ts$ [yr]). Low weathering zone ages, for instance, are indicative of fast supply of fresh
210    minerals, resulting in higher reaction rates, and consequently reduced kinetic limitation. Many
211    catchments today have concentrations that are invariant to changes in runoff (*i.e.*, chemostatic;
212    Godsey et al., 2009), suggesting that kinetic-limitation may not be widespread. Lastly, soil
213    $pCO_2$ modifies the maximum equilibrium $[C]_{sil}$ ($[C]_{sil,eq}$), and we assume an open weathering
214    zone $CO_2$ system (Winnick & Maher, 2018), which is a reasonable assumption given that plants
215    and microbes continually supply $CO_2$ to the weathering zone via root and soil respiration. We
216    assume that soil $pCO_2$ scales—via a Michaelis-Menton relationship—to changes in
217    atmospheric $pCO_2$ that increase aboveground gross primary productivity (Volk, 1987).
218    Assuming a linear scaling between soil $CO_2$ and atmospheric $CO_2$ does not substantially alter
219    the conclusions presented here. This set of equations permits us to constrain $[C]_{sil}$ as a function
220    of several climatic parameters (*i.e.*, temperature ($T$), $CO_2$, and $q$) and the weathering zone
221    reactivity and, therefore, treat $q$-sensitivity as the main unknown parameter.
222
223    *2.2 Projected changes in runoff*
224         To compare our CH2O-CHOO model results with state-of-the-art Earth system model
225    projections of global $q$ change, we interrogate those models that participated in the C4MIP
226    experiments (Table S2) (Arora et al., 2013, 2020). These model versions account for a more
227    elaborate representation of land processes, such as the response of evapotranspiration to
228    warming and rising $CO_2$. We calculate the ensemble mean runoff sensitivity to warming (%/K)
229    in the 1pctCO2 experiments (1% annual increase in atmospheric $CO_2$) across CMIP5 and
230    CMIP6 models. For each model, we estimate the relative $q$-sensitivity by linearly regressing
231    the change in $q$ against the change in temperature. We find that, while the spatial distribution
232    of $q$ change is patchy and there is poor model agreement across much of the land surface, the
233    ensemble average global $q$-sensitivity is $3.1 \pm 0.9\%$, driven by an increase in $P$ and a slight
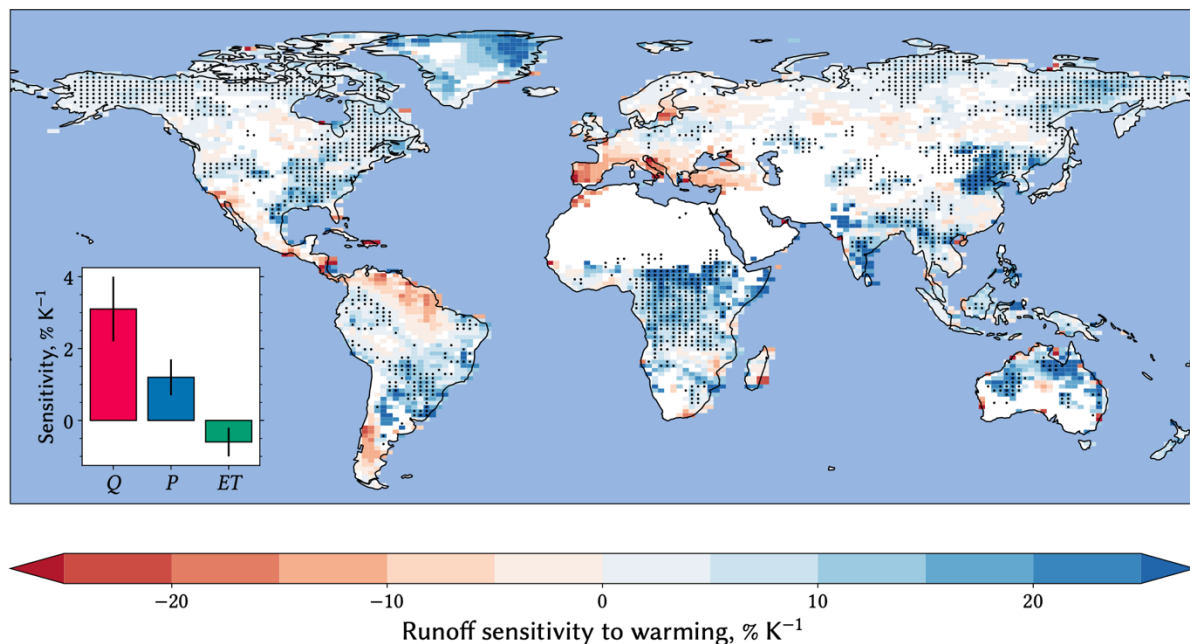234    decrease in $ET$ (Figure 2).
235

*Figure 2*: The *q*-sensitivity (%/K) averaged across the C4MIP models (combined CMIP5 and CMIP6). Stippling indicates where at least 75% of the models (6 of 8) agree on the sign of the runoff sensitivity. Inset shows the globally-averaged *q*-, *P*-, and *ET*-sensitivity (%/K)

## 3. Carbon Cycle Constraints on Runoff Changes with Warming

To estimate how differences in the sensitivity of runoff with warming (*i.e.*, the *q*-sensitivity) affect the long-term carbon cycle, we again use CH2O-CHOO and inject 1000 Pg of carbon into the ocean-atmosphere over the span of 100 years and permit long-term carbon cycle processes to restore atmospheric $CO_2$ to pre-perturbation conditions. Here, we treat the *q*-sensitivity as an independent variable; however, unlike in the example above, $[C]_{sil}$ is now constrained via its relationship to atmospheric $CO_2$ through $T$, $q$, and soil $pCO_2$ (Maher & Chamberlain, 2014; Volk, 1987; Winnick & Maher, 2018). We test cases where *(1)* we vary $T_s$ between 10,000 and 100,000 years (the average weathering zone age today is 20,000; Larsen et al., 2014); *(2)* $[C]_{sil}$ is constant, following indications that many catchments on short timescales are chemostatic (Godsey et al., 2009; Ibarra et al., 2016); *(3)* seafloor weathering— which is dependent only upon bottom-water temperatures and not upon $q$ (Brady & Gíslason, 1997; Coogan & Gillis, 2018)—represents 20% of the pre-perturbation weathering flux (Hilton & West, 2020), and; *(4)* silicate weathering rates are predicted using a different model, from West (2012), which also contains terms for $q$, $T$, and land surface reactivity.

Though the precise recovery time [yr] for $CO_2$ at a given *q*-sensitivity varies depending upon the value of the weathering parameters, in all cases, the timescale for atmospheric $CO_2$

258  to return to pre-perturbation values decreases as the $q$-sensitivity increases. This is perhaps
259  most easily shown by the case of constant concentrations (blue line, Figure 3). In this case,
260  $[C]_{sil}$ remains constant as $CO_2$ changes and is unaffected by changes in $q$, $T$, or $pCO_2$;
261  consequently, recovery from a perturbation is impossible once the $q$-sensitivity falls below
262  0%/K, given the relationship in Eq. 1. Indeed, even where $[C]_{sil}$ is constant, recovery timescales
263  surpass 1 Ma for $q$-sensitivities below $\sim$ 2.5%/K. In all other cases, both $q$ and $[C]_{sil}$ are
264  permitted to vary as atmospheric $CO_2$ changes; yet, even in these other experiments, recovery
265  times surpass 1 Ma at or near a $q$-sensitivity of 0%/K. This result arises because, though both
266  $q$ and $[C]_{sil}$ are linearly related to $F_{silw}$ (Eq. 2), changes in $[C]_{sil}$ are typically smaller than
267  changes in $q$ as atmospheric $CO_2$ changes (Figure S1), resulting in a greater influence of $q$ on
268  the ultimate recovery from a C-cycle perturbation. While this supposition is based upon our
269  model of weathering, decreases in $[C]_{sil}$ do not follow perfect dilution trajectories as $q$
270  increases, as seen in datasets that reflect short-term (Godsey et al., 2009) and long-term
271  processes (Godsey et al., 2019; Li et al., 2022), further supporting the idea that variations in
272  $q$—and not in $[C]_{sil}$—are the dominant control on $F_{silw}$.

273        The critical influence of $q$ can be seen in how different parameterizations affect the
274  recovery time. As weathering zone age increases, the recovery time increases for a given $q$-
275  sensitivity because $[C]_{sil}$ becomes insensitive to changes in $q$, due to the relative decrease in
276  weathering zone reactivity. Similarly, if 20% of the initial, global $F_{silw}$ occurs due to seafloor
277  basalt weathering (green line), recovery times are slightly shorter for a given $q$-sensitivity,
278  because a portion of $[C]_{sil}$—that generated by seafloor weathering—is insensitive to changes
279  in $q$ and only sensitive to changes in $T$. Below a $q$-sensitivity of 0%/K, seafloor weathering
280  begins to substantially reduce recovery times because $T$ rises far more in response to the carbon
281  cycle perturbation due to the reduction in weathering on land, causing seafloor weathering to
282  become a greater proportion of total $F_{silw}$. The West (2012) formulation (red line) posits a faster
283  recovery time for most $q$-sensitivities, largely because $F_{silw}$ is formulated not as a linear
284  combination of $q$ and $[C]_{sil}$ but rather as linearly dependent upon erosion rate, which is
285  presumed to be independent of climate. This linear sensitivity to erosion rate yields a strong
286  dependence upon land surface reactivity that helps to decouple $F_{silw}$ from changes in $q$.
287  Nevertheless, as in the model of Maher and Chamberlain, if erosion rate decreases (equivalent
288  to an increase in the weathering zone age), the West (2012) model predicts longer recovery
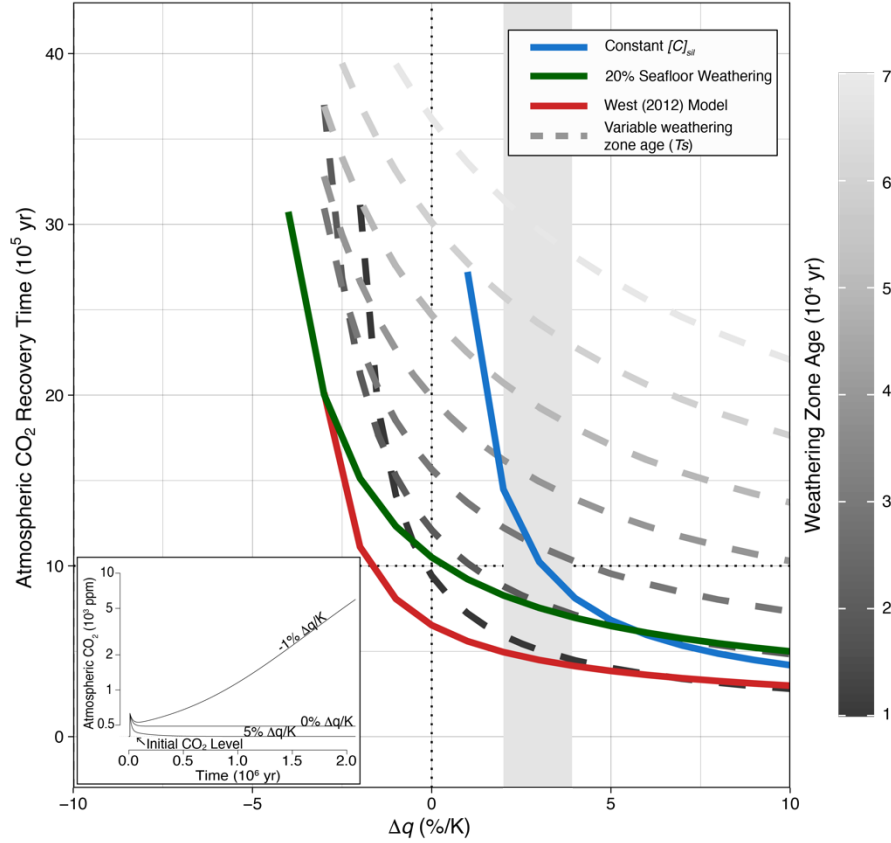289  times for equivalent $q$-sensitivities (Figure S2).

290

*Figure 3*: Recovery time [$10^5$ yr] for atmospheric $CO_2$ as a function of the $q$-sensitivity (%/K) given a 1000 Pg C-cycle perturbation over 100 years. Dashed, gray lines use the standard parameters in Table S1 and variable $Ts$; blue line assumes globally chemostatic catchments (*i.e.*, [C]$_{sil}$ is invariant with changes in $CO_2$); green line assumes that seafloor weathering accounts for 20% of the total alkalinity flux to the ocean (with all other parameters derived from Table S1); red line uses the silicate weathering model of West (2012) using values from Table S1. Vertical gray bar is the range of $q$-sensitivity from the C4MIP models considered herein. Inset shows atmospheric $CO_2$ (log-scale) of three representative experiments from the case of invariant [C]$_{sil}$ (blue line). Given a -1% $q$-sensitivity, atmospheric $CO_2$ increases in perpetuity. With 0% $q$-sensitivity, atmospheric $CO_2$ stabilizes but does not recover to pre-perturbation conditions. A $q$-sensitivity of 5% results in recovery to pre-perturbation $CO_2$ within ~ 700 kyr.

The above analysis suggests that, for the ocean-atmosphere system to recover to pre-perturbation $CO_2$ within 1 Ma, $q$-sensitivity must be greater than -2 %/K for any conceivable combination of weathering parameters; depending upon the precise model and parameterization, this value may be higher. For example, our preferred model of weathering—

308    using Maher and Chamberlain (2014)—requires a $q$-sensitivity of > 0 %/K for all reasonable
309    estimates of the global weathering zone age.

310        However, the above modeling results assume that the Earth's surface can be
311    characterized by single, mean values; such an assumption is likely incorrect. For example,
312    while the C4MIP ensemble global-mean $q$-sensitivity is 3.1 ± 0.9 %/K (similar to the CMIP5
313    ensemble mean; Zhang et al., 2014), the spatial variability across large catchments is enormous,
314    spanning -20 to +40 %/K (Dai & Trenberth, 2002; Scheff et al., 2017; Swann et al., 2016)
315    (Figure 2). High, regional $q$-sensitivity may coincide with particularly reactive rocks (*i.e.*, low
316    weathering zone ages and consequently high $[C]_{sil}$-sensitivity) yielding a different $CO_2$
317    recovery time due to spatial co-variability in weathering zone reactivity and runoff change.
318    Indeed, consistently high tropical runoff is the basis for theories that posit that exposure of
319    reactive rocks (such as ophiolites or exposure of Large Igneous Province basalts) near the
320    equator is the primary mode of long-term atmospheric $CO_2$ control (Donnadieu et al., 2004;
321    Macdonald et al., 2019; Park et al., 2020; Swanson-Hysell & Macdonald, 2017).

322        Consequently, our estimate of the minimum $q$-sensitivity may be biased high because
323    we do not consider regions with coincident high $q$-sensitivity and high weathering zone
324    reactivity. To test this possibility, we modify CH2O-CHOO such that two distinct regions
325    contribute toward the global silicate weathering flux: Mountain Region consists of a highly
326    reactive weathering zone ($Ts$ = 1000 yr) and contributes 50% of the initial, pre-perturbation
327    global $F_{silw}$ and Lowland Region comprises the rest of the world and is characterized by low
328    weathering zone reactivity ($Ts$ = 39,000 yr). Though this example is simplified, the Mountain
329    Region may be considered equivalent to the role of mountains today, which contribute half of
330    the global weathering flux (silicate and carbonate weathering combined) (Larsen et al., 2014).
331    We treat the Mountain Region as having a fixed, positive $q$-sensitivity and the Lowland Region
332    as having variable $q$-sensitivity. Globally, the $q$-sensitivity of mountains more likely tracks
333    changes in $P$ than changes in $ET$ because most precipitation in mountain ranges is partitioned
334    to $q$. In general, mountain ranges—particularly coastal ones—witness changes in $P$ similar to
335    the zonal mean, such that subtropical ranges see declines in $P$ (and likely $q$), whereas mid-
336    latitude ranges may see changes in $P$ equal to or greater than 7 %/K (Shi & Durran, 2014). We
337    repeat the experiment above, treating the $q$-sensitivity of the Low-Land Region as an
338    independent parameter and injecting 1000 Pg C into the ocean-atmosphere system over 100
339    years. We test two cases: *(1)* where the Mountain Region has a fixed $q$-sensitivity of 3%/K and
340    *(2)* where the Mountain Region has a fixed $q$-sensitivity of 6%/K.

341        Even the coincidence of high weathering zone reactivity with high runoff sensitivity

342    still requires that average global runoff sensitivity be > 0%/K in order for atmospheric $CO_2$ to

343    recover to pre-perturbation levels within ~ 1 Ma (Figure 4). Though a greater Mountain Region

344    $q$-sensitivity (6 vs. 3 %/K) results in faster recovery times, the minimum $q$-sensitivity is still 0

345    %/K to recover from a perturbation within 1 Myr. The different relationship between $\Delta q$ and

346    recovery time and compressed $\Delta q$ variability in these simulations is due to how $\Delta q$ is calculated

347    for this experiment; in contrast to the first experiments above, where $\Delta q$ is prescribed, here

348    50% of the Earth experiences a fixed 3 or 6 %/K $q$-sensitivity. Though we vary the $q$-sensitivity

349    for the Lowland region (*i.e.*, with low weathering zone reactivity and high $Ts$), variations in

350    global $\Delta q$ are damped, given the fixed $q$-sensitivity in the Mountain Region (*i.e.* with high

351    weathering zone reactivity and low $Ts$). Further, any decreases in global $q$ when the $q$-

352    sensitivity of the Lowland Region is < 0%/K are small (see inset in Figure 2) and global average

353    $[C]_{sil}$ increases due to the effect of rising temperatures that offset the small decrease in $q$.
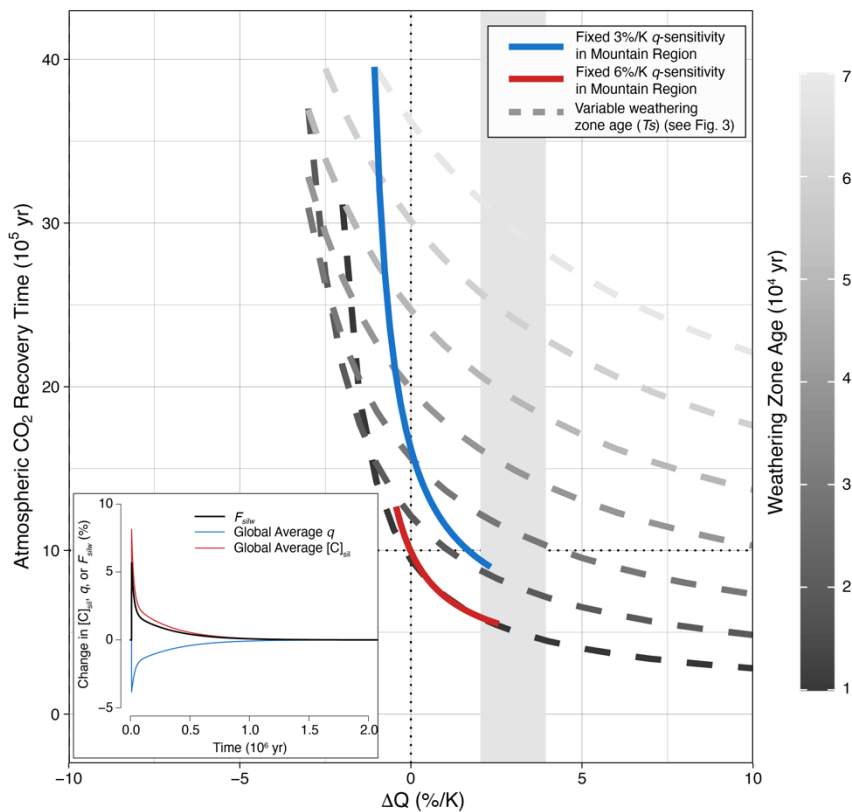


354

355

356    *Figure 4*: Recovery time [$10^5$ y] for atmospheric $CO_2$ as a function of the average $q$-sensitivity

357    (%/K) given a 1000 Pg C-cycle perturbation over 100 years and two distinct weathering regions

358    (outlined in text). Dashed lines use the standard parameters in Table S1 with variable

359    weathering zone age ($Ts$) (see Figure 3); solid, red line assumes a fixed Mountain Region $q$-

360  sensitivity of 6 %/K; solid, blue line assumes a fixed Mountain Region $q$-sensitivity of 3%/K.

361  In both cases, the $q$-sensitivity of region 2 is permitted to vary between -10 and 10 %/K. Gray

362  shading is the C4MIP estimate of runoff sensitivity. We calculate $\Delta q$ as the percentage change

363  in global $q$ at the peak of the C-cycle perturbation relative to starting global $q$ against the change

364  in global $T$ between the peak of the perturbation and the initial condition. Inset shows how $F_{silw}$

365  (black line), global average $q$ (blue line), and global average $[C]_{sil}$ (red line) change during a

366  perturbation when the Lowland Region has a -10 %/K $q$-sensitivity and the Mountain Region

367  has a low $Ts$ (ie, highly reactive) and a fixed $q$-sensitivity of 6 %/K.

368

369  **4. Geologic Constraints on q-sensitivity**

370  We now use a well-studied past large carbon cycle perturbation—the Paleocene-Eocene

371  Thermal Maximum (PETM), ~ 55Ma—to constrain the $q$ response to a large carbon cycle

372  perturbation. Though the exact cause of the PETM remains debated, a substantial quantity of

373  carbon (5000-20000 Pg C) was released to the ocean-atmosphere system within 3000–10000

374  years, lowering global marine dissolved inorganic carbon (DIC) $\delta^{13}C$ by 3–4‰ (Cui et al.,

375  2011; Gutjahr et al., 2017; Panchuk et al., 2008; Penman et al., 2016). This negative carbon

376  isotope excursion is thought to have lasted ~ 170 ± 30 ka (Zeebe & Lourens, 2019), at which

377  point the global marine DIC pool had recovered to pre-perturbation $\delta^{13}C$ values. Critically, the

378  recovery from the PETM was likely mediated by silicate weathering—as evidenced by an

379  excess burial of Si across the PETM (Penman, 2016)—and involved large-scale increases in

380  runoff in places (Chen et al., 2018; Foreman et al., 2012). The PETM thus provides an

381  opportunity to test our CH2O-CHOO model and determine the most likely $q$-sensitivity

382  necessary to match the duration of the $\delta^{13}C$ negative excursion.

383  We force CH2O-CHOO with net carbon emissions and net emissions $\delta^{13}C$ estimates

384  from Gutjahr et al. (2017), which also includes estimates of increased organic carbon burial

385  during the recovery phase (Bowen, 2013; Bowen & Zachos, 2010). As before, we prescribe a

386  wide-range of $q$-sensitivity estimates that determine how runoff responds to changes in

387  atmospheric $CO_2$. Because we also do not *a priori* know the average weathering zone age ($Ts$)

388  at the PETM, we vary this parameter as well, though evidence from a range of carbon cycle

389  models and isotopic data indicates that bulk Earth surface weatherability was lower in the early

390  Eocene, likely reflecting higher $Ts$ (Caves et al., 2016; Froelich & Misra, 2014; Krissansen-

391  Totton & Catling, 2017; van der Ploeg et al., 2018; Vervoort et al., 2021).

392    Given these constraints, we find that, to match the duration of the PETM negative $\delta^{13}C$
393    excursion requires $q$-sensitivity to be equal to or greater than 0%/K if $Ts$ is similar to today
394    (Figure 5). If, instead, $Ts$ was higher in the late Paleocene, then $q$-sensitivity must be higher to
395    match the duration of the $\delta^{13}C$ negative excursion. Though our model lacks a number of critical
396    carbon cycle processes that are thought to modulate the impact of rapid $CO_2$ emissions (such
397    as seafloor carbonate sediments that buffer against acidic bottom waters), these effects are
398    likely to matter primarily for the initial stages of the perturbation, rather than mediating the
399    long-term removal of $CO_2$ by silicate weathering (Penman et al., 2020). We note that, while
400    the PETM provides a useful analogue with which to understand how $q$ responds to $CO_2$, we do
401    not expect the $q$-sensitivity at the PETM to exactly match that of today's Earth, due to
402    paleogeographic and floral changes that have occurred during the Cenozoic that would have
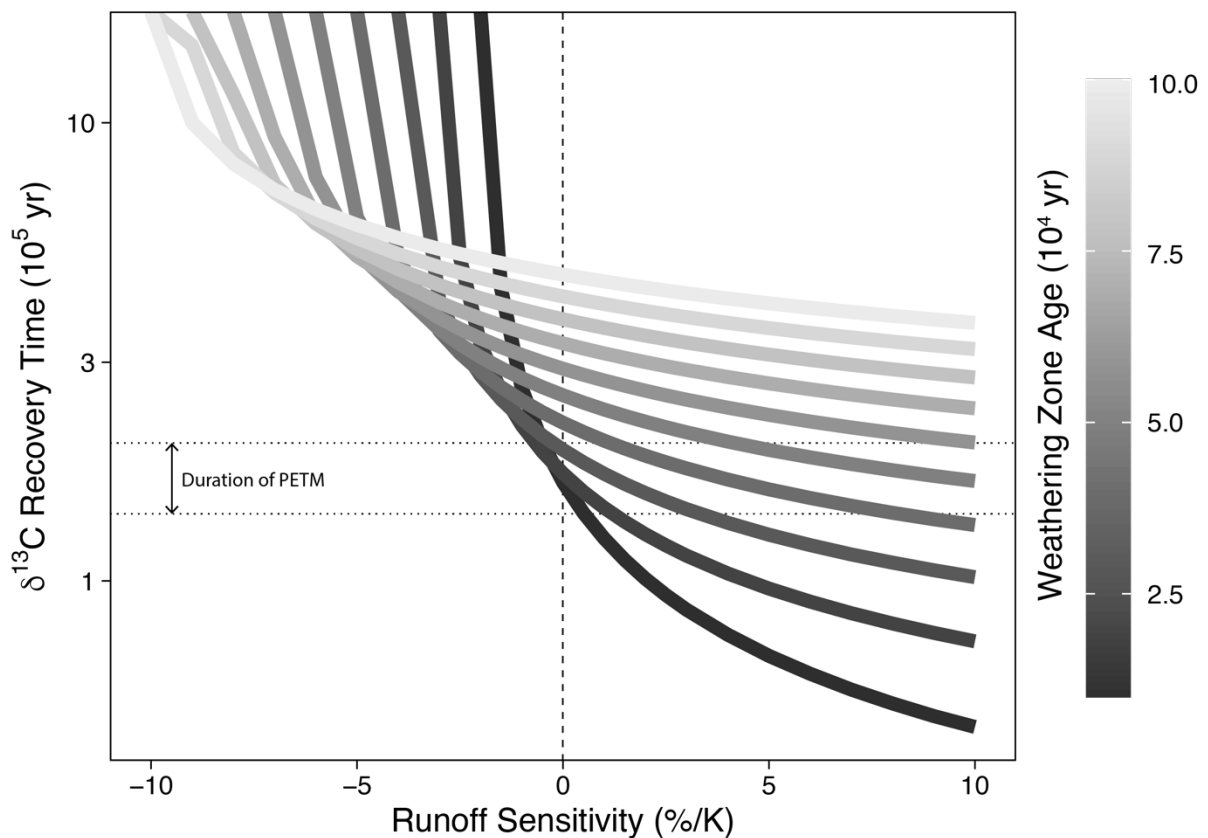403    changed precisely how much precipitation is converted to $q$ as $CO_2$ rises.

404



405

406

407    *Figure* 5: Estimated $\delta^{13}C$ recovery times ($10^5$ yr) as a function of the $q$-sensitivity and the
408    weathering zone age (grayscale). Horizontal dotted lines indicate the estimated $\delta^{13}C$ recovery
409    time based upon astrochronological tuning of the PETM $\delta^{13}C$ record (Zeebe & Lourens, 2019).

410

## 5. Implications

The geological record—and our understanding of how the Earth recovers from carbon cycle perturbations—provides long-term constraints on how $q$ must respond to increases in atmospheric $CO_2$. In a broad sense, our results bolster previous work pointing towards the importance of runoff in modulating the long-term carbon cycle and climate (Barron et al., 1989; François & Walker, 1992; Otto-Bliesner, 1995). Critically, our long-term perspective on the runoff response to $CO_2$ incorporates a number of processes that are thought to affect $q$ but are difficult to constrain in the modern due to temporally limited instrumental records or experiments. For example, remotely sensed products of global discharge are affected by internal variability, which precludes their use currently in assessing how total runoff will respond to rising atmospheric $CO_2$ (Chandanpurkar et al., 2017, 2021). Experiments that seek to understand how plant responses might affect runoff—such as the Free Air $CO_2$ Enrichment (FACE) experiments—are relatively short-term and the long-term response of ecosystems may differ from the short-term response due to changes in nutrient demands and supply and non-linear plant responses to increasing $CO_2$. In this sense, the known response of the long-term carbon cycle—and how this response is linked to $q$—provides a constraint on how global $q$ must respond to rising $CO_2$ that avoids the inherent noisiness of the relatively short instrumental record.

Our finding that $q$-sensitivity must be greater than or equal to 0%/K (when using our preferred model of weathering) holds implications for the processes that control changes in runoff with warming. Though $PET$ should increase faster than $P$, stomatal conductance changes driven by $CO_2$ fertilization and increasing vapor pressure deficits may result in a greater fraction of $P$ being partitioned to $q$ (Novick et al., 2016; Roderick et al., 2015; Swann et al., 2016). This effect, however, is complicated by a number of factors that may instead drive greater plant water use, including a longer growing season (Mankin et al., 2019) and widespread greening that increases total leaf area (Zhu et al., 2016). How these factors will interact across the planet to produce a change in global $q$ remains difficult to predict; across much of the Earth's surface, for example, models frequently do not even agree on the sign of the $q$ change (Figure 2). For example, in much of the mid-latitudes, projected ensemble mean runoff changes are negligible, with little model agreement on the sign of the change (Elbaum et al., 2022; Scheff et al., 2017). Our results suggest that the processes on a global scale that tend towards greater $q$ with increasing atmospheric $CO_2$ and warming—such as reductions in stomatal conductance—will be predominant in a warmer world, though there may be substantial spatial variability. Further, we note that our results likely hold on the millennial or

445 longer timescale, and, as such and given the potential complexity of the biospheric response to
446 warming, there may be long periods when global runoff may not increase in response to
447 warming.

448        Our findings also hold implications for understanding how paleogeographic changes
449 may have modified the strength of the silicate weathering negative feedback in the geologic
450 past. General circulation model simulations highlight that the runoff response to warming is
451 spatially complex; such results indicate the precise global $q$-sensitivity may vary with the
452 position of the continents (Otto-Bliesner, 1995). For example, models frequently predict that
453 subtropical areas should become drier (Burls & Fedorov, 2017; Mankin et al., 2019),
454 suggesting that a world with predominantly sub-tropical continents would perhaps see a
455 minimal increase or even decrease in global discharge. Our results suggest that either there are
456 additional mechanisms that keep global discharge from decreasing or that such a continental
457 configuration has never occurred on Earth during a major carbon cycle perturbation. If such an
458 Earth experienced a major perturbation, our results indicate that atmospheric $CO_2$ may have
459 never returned to pre-perturbation values.

460        Though we have attempted to test the robustness of our result by using different
461 parameters and even a different model of weathering (West, 2012), there are a number of
462 hypothesized feedbacks with warming and rising $CO_2$ that may impact weathering fluxes, but
463 are not—to our knowledge—yet incorporated into any model of weathering. For example,
464 warming is thought to increase the number of extreme precipitation events (Fischer & Knutti,
465 2016) which is likely to increase $q$ relative to $ET$ as $P$ is rapidly converted to $q$. Though $q$
466 increases with these extreme events, much of the water may bypass the weathering zone,
467 limiting their impact on weathering. In turn, extreme events may also increase erosional
468 efficiency (Deal et al., 2017, 2018), increasing the availability of fresh minerals and thereby
469 enhancing silicate weathering by reducing average $Ts$. Though this process is not represented
470 in our model, we suspect that the impact of extreme events on silicate weathering is likely to
471 be minimal, as lower $Ts$ is offset by a greater quantity of $q$ that bypasses the weathering zone
472 via overland flow or exceptionally fast transit times. Additionally, other carbon fluxes may
473 change with a warming climate, such as erosion and burial of terrestrial organic carbon (Hilton,
474 2017) or increases in marine organic burial due to widespread anoxia (Lau et al., 2016).
475 However, these mechanisms also rely upon runoff to transport terrestrial organic matter to
476 continental shelves for burial and to delivery sufficient nutrients to drive marine anoxia (Them
477 et al., 2017), suggesting that increases in runoff are also necessary for these hypothesized
478 negative feedbacks on $CO_2$.

479    Our work highlights the tight coupling between the hydrological cycle and the long-
480    term carbon cycle and demonstrates that this coupling places a lower-bound on the globally
481    averaged runoff response to warming and rising $CO_2$. Whereas abundant research has
482    examined the links between the hydrological cycle and the short-term carbon cycle (Forzieri et
483    al., 2020; Lemordant et al., 2018; Novick et al., 2016), our work demonstrates that the operation
484    of the long-term carbon cycle is also critically linked to the hydrological cycle. It is this linkage
485    that has acted to remove excess $CO_2$ from the ocean-atmosphere system during perturbations,
486    thus maintaining Earth's habitability. Though our knowledge of weathering continues to
487    improve, ongoing model and observational work indicates the centrality of runoff in linking
488    the weathering of silicate rocks to the ultimate burial of carbon as calcium carbonate in the
489    marine environment. Thus, the importance of runoff for weathering indicates that, on long
490    timescales, runoff must increase as $CO_2$ rises.
491

501

502    **Software Availability Statement**:
503    Model source code used for this research is available in Rugenstein and Winkler (2022) and
504    can be accessed at: https://doi.org/10.5281/zenodo.7219627.

**References**:

Arora, V. K., Boer, G. J., Friedlingstein, P., Eby, M., Jones, C. D., Christian, J. R., et al. (2013). Carbon-concentration and carbon-climate feedbacks in CMIP5 earth system models. *Journal of Climate*, *26*(15), 5289–5314. https://doi.org/10.1175/JCLI-D-12-00494.1

Arora, V. K., Katavouta, A., Williams, R. G., Jones, C. D., Brovkin, V., Friedlingstein, P., et al. (2020). Carbon – concentration and carbon – climate feedbacks in CMIP6 models and their comparison to CMIP5 models. *Biogeosciences*, *17*, 4173–4222.

Barron, E. J., Hay, W. W., & Thompson, S. (1989). The hydrologic cycle: A major variable during earth history. *Palaeogeography, Palaeoclimatology, Palaeoecology*, *75*(3), 157–174. https://doi.org/10.1016/0031-0182(89)90175-2

Baum, M., Fu, M., & Bourguet, S. (2022). Sensitive Dependence of Global Climate to Continental Geometry. *Geophysical Research Letters*, *49*(11), 1–8. https://doi.org/10.1029/2022gl098843

Berner, R. A., & Kothavala, Z. (2001). GEOCARB III: A revised model of atmospheric $CO_2$ over Phanerozoic time. *American Journal of Science*, *301*, 182–204. Retrieved from http://ajsonline.org/content/301/2/182.short

Berner, Robert A., & Caldeira, K. (1997). The need for mass balance and feedback in the geochemical carbon cycle. *Geology*, *25*(10), 955–956. https://doi.org/10.1130/0091-7613(1997)025<0955:TNFMBA>2.3.CO;2

Bowen, G. J. (2013). Up in smoke: A role for organic carbon feedbacks in Paleogene hyperthermals. *Global and Planetary Change*, *109*, 18–29. https://doi.org/10.1016/j.gloplacha.2013.07.001

Bowen, G. J., & Zachos, J. C. (2010). Rapid carbon sequestration at the termination of the Palaeocene–Eocene Thermal Maximum. *Nature Geoscience*, *3*(12), 866–869. https://doi.org/10.1038/ngeo1014

Brady, P. V., & Gíslason, S. R. (1997). Seafloor weathering controls on atmospheric $CO_2$ and global climate. *Geochimica et Cosmochimica Acta*, *61*(5), 965–973. https://doi.org/10.1016/S0016-7037(96)00385-7

Burls, N. J., & Fedorov, A. V. (2017). Wetter subtropics in a warmer world: Contrasting past and future hydrological cycles. *Proceedings of the National Academy of Sciences*, *114*(49), 12888–12893. https://doi.org/10.1073/pnas.1703421114

Caves, J. K., Jost, A. B., Lau, K. V., & Maher, K. (2016). Cenozoic carbon cycle imbalances and a variable silicate weathering feedback. *Earth and Planetary Science Letters*, *450*,

539       152–163. https://doi.org/10.1016/j.epsl.2016.06.035

540    Caves Rugenstein, J. K., Ibarra, D. E., & von Blanckenburg, F. (2019). Neogene cooling

541       driven by land surface reactivity rather than increased weathering fluxes. *Nature*, *571*,

542       99–102. https://doi.org/10.1038/s41586-019-1332-y

543    Chandanpurkar, H. A., Reager, J. T., Famiglietti, J. S., & Syed, T. H. (2017). Satellite- and

544       reanalysis-based mass balance estimates of global continental discharge (1993-2015).

545       *Journal of Climate*, *30*(21), 8481–8495. https://doi.org/10.1175/JCLI-D-16-0708.1

546    Chandanpurkar, H. A., Reager, J. T., Famiglietti, J. S., Nerem, R. S., Chambers, D. P., Lo, M.

547       H., et al. (2021). The Seasonality of Global Land and Ocean Mass and the Changing

548       Water Cycle. *Geophysical Research Letters*, *48*(7).

549       https://doi.org/10.1029/2020GL091248

550    Chen, C., Guerit, L., Foreman, B. Z., Hassenruck-Gudipati, H. J., Adatte, T., Honegger, L., et

551       al. (2018). Estimating regional flood discharge during Palaeocene-Eocene global

552       warming. *Scientific Reports*, *8*(1), 1–8. https://doi.org/10.1038/s41598-018-31076-3

553    Colbourn, G., Ridgwell, A., & Lenton, T. M. (2015). The time scale of the silicate weathering

554       negative feedback on atmospheric $CO_2$. *Global Biogeochemical Cycles*, *29*, 583–596.

555       https://doi.org/10.1002/2014GB005054

556    Coogan, L. A., & Gillis, K. M. (2018). Low-Temperature Alteration of the Seafloor: Impacts

557       on Ocean Chemistry. *Annu. Rev. Earth Planet. Sci*, *46*, 21–45.

558       https://doi.org/10.1146/annurev-earth-082517

559    Cook, B. I., Smerdon, J. E., Seager, R., & Coats, S. (2014). Global warming and 21st century

560       drying. *Climate Dynamics*, *43*, 2607–2627. https://doi.org/10.1007/s00382-014-2075-y

561    Cui, Y., Kump, L. R., Ridgwell, A. J., Charles, A. J., Junium, C. K., Diefendorf, A. F., et al.

562       (2011). Slow release of fossil carbon during the Palaeocene–Eocene Thermal Maximum.

563       *Nature Geoscience*, *4*(7), 481–485. https://doi.org/10.1038/ngeo1179

564    Dai, A., & Trenberth, K. E. (2002). Estimates of Freshwater Discharge from Continents :

565       Latitudinal and Seasonal Variations. *Journal of Hydrometeorology*, *3*, 660–687.

566    Deal, E., Favre, A.-C., & Braun, J. (2017). Rainfall variability in the Himalayan orogen and

567       its relevance to erosion processes. *Water Resources Research*, *53*, 4004–4021.

568       https://doi.org/10.1002/2013WR014979.Reply

569    Deal, E., Botter, G., & Braun, J. (2018). Understanding the role of rainfall and hydrology in

570       determining fluvial erosion efficiency. *Journal of Geophysical Research: Earth Surface*.

571       https://doi.org/10.1002/2017JF004393

572    Donnadieu, Y., Goddéris, Y., Ramstein, G., Nédélec, A., & Meert, J. (2004). A 'snowball

573     Earth' climate triggered by continental break-up through changes in runoff. *Nature*,

574     *428*(6980), 303–306. https://doi.org/10.1038/nature02408

575 Douville, H., Raghavan, K., Renwick, J., Allan, R. P., Arias, P. A., Barlow, M., et al. (2021).

576     Water Cycle Changes. In V. Masson-Delmotte, P. Zhai, A. Pirani, S. L. Connors, C.

577     Péan, S. Berger, et al. (Eds.), *Climate Change 2021: The Physical Science Basis.*

578     *Contribution of Working Group I to the Sixth Assessment Report of the*

579     *Intergovernmental Panel on Climate Change* (p. 239). Cambridge University Press.

580 Elbaum, E., Garfinkel, C. I., Adam, O., Morin, E., Rostkier-Edelstein, D., & Dayan, U.

581     (2022). Uncertainty in projected changes in precipitation minus evaporation: Dominant

582     role of dynamic circulation changes and weak role for thermodynamic changes.

583     *Geophysical Research Letters*. https://doi.org/10.1029/2022gl097725

584 Ficklin, D. L., & Novick, K. A. (2017). Historic and projected changes in vapor pressure

585     deficit suggest a continental-scale drying of the United States atmosphere. *Journal of*

586     *Geophysical Research: Atmospheres*, *122*, 2061–2079.

587     https://doi.org/10.1002/2016JD025855

588 Fischer, E. M., & Knutti, R. (2016). Observed heavy precipitation increase confirms theory

589     and early models. *Nature Climate Change*, *6*(11), 986–991.

590     https://doi.org/10.1038/nclimate3110

591 Foreman, B. Z., Heller, P. L., & Clementz, M. T. (2012). Fluvial response to abrupt global

592     warming at the Palaeocene/Eocene boundary. *Nature*, 1–4.

593     https://doi.org/10.1038/nature11513

594 Forzieri, G., Miralles, D. G., Ciais, P., Alkama, R., Ryu, Y., Duveiller, G., et al. (2020).

595     Increased control of vegetation on global terrestrial energy fluxes. *Nature Climate*

596     *Change*, *10*. https://doi.org/10.1038/s41558-020-0717-0

597 François, L. M., & Walker, J. C. G. (1992). Modelling the Phanerozoic carbon cycle and

598     climate: constraints from the 87Sr/86Sr isotopic ratio of seawater. *American Journal of*

599     *Science*. https://doi.org/10.2475/ajs.292.2.81

600 Froelich, F., & Misra, S. (2014). Was the late Paleocene-early Eocene hot because Earth was

601     flat? An ocean lithium isotope view of mountain building, continental weathering,

602     carbon dioxide, and Earth's Cenozoic climate. *Oceanography*, *27*(1), 36–49. Retrieved

603     from http://eprints.esc.cam.ac.uk/2999/

604 Godsey, S. E., Kirchner, J. W., & Clow, D. W. (2009). Concentration – discharge

605     relationships reflect chemostatic characteristics of US catchments. *Hydrological*

606     *Processes*, *23*, 1844–1864. https://doi.org/10.1002/hyp

607 Godsey, S. E., Hartmann, J., & Kirchner, J. W. (2019). Catchment chemostasis revisited:
608     Water quality responds differently to variations in weather and climate. *Hydrological*
609     *Processes*, 1–14. https://doi.org/10.1002/hyp.13554

610 Good, S. P., Noone, D., & Bowen, G. (2015). Hydrologic connectivity constrains partitioning
611     of global terrestrial water fluxes. *Science*, *349*(6244), 175–177.

612 Graham, R. J., & Pierrehumbert, R. T. (2020). Thermodynamic and Energetic Limits on
613     Continental Silicate Weathering Strongly Impact the Climate and Habitability of Wet,
614     Rocky Worlds. Retrieved from http://arxiv.org/abs/2004.14058

615 Gutjahr, M., Ridgwell, A., Sexton, P. F., Anagnostou, E., Pearson, P. N., Pälike, H., et al.
616     (2017). Very large release of mostly volcanic carbon during the Palaeocene–Eocene
617     Thermal Maximum. *Nature*, *548*(7669), 573–577. https://doi.org/10.1038/nature23646

618 Held, I., & Soden, B. (2006). Robust responses of the hydrological cycle to global warming.
619     *Journal of Climate*, *19*, 5686–5699.

620 Hilton, R. G. (2017). Climate regulates the erosional carbon export from the terrestrial
621     biosphere. *Geomorphology*, *277*, 118–132.
622     https://doi.org/10.1016/j.geomorph.2016.03.028

623 Hilton, R. G., & West, A. J. (2020). Mountains, erosion and the carbon cycle. *Nature Reviews*
624     *Earth and Environment*. Springer US. https://doi.org/10.1038/s43017-020-0058-6

625 Ibarra, D. E., Caves, J. K., Moon, S., Thomas, D. L., Hartmann, J., Chamberlain, C. P., &
626     Maher, K. (2016). Differential weathering of basaltic and granitic catchments from
627     concentration–discharge relationships. *Geochimica et Cosmochimica Acta*, *190*, 265–
628     293. https://doi.org/10.1016/j.gca.2016.07.006

629 Knutti, R., Rugenstein, M. A. A., & Hegerl, G. C. (2017). Beyond equilibrium climate
630     sensitivity. *Nature Geoscience*, *10*, 727–736. https://doi.org/10.1038/ngeo3017

631 Krissansen-Totton, J., & Catling, D. C. (2017). Constraining climate sensitivity and
632     continental versus seafloor weathering using an inverse geological carbon cycle model.
633     *Nature Communications*, *8*, 15423. https://doi.org/10.1038/ncomms15423

634 Kump, L. R., & Arthur, M. A. (1999). Interpreting carbon-isotope excursions: carbonates and
635     organic matter. *Chemical Geology*, *161*(1–3), 181–198. https://doi.org/10.1016/S0009-
636     2541(99)00086-8

637 Kump, L. R., Brantley, S. L., & Arthur, M. A. (2000). Chemical weathering, atmospheric
638     $CO_2$, and climate. *Annual Review of Earth and Planetary Sciences*, *28*, 611–667.
639     Retrieved from http://www.annualreviews.org/doi/abs/10.1146/annurev.earth.28.1.611

640 Larsen, I. J., Montgomery, D. R., & Greenberg, H. M. (2014). The contribution of mountains

to global denudation. *Geology*, *42*, 527–530. https://doi.org/10.1130/G35136.1

Lau, K. V., Maher, K., Altiner, D., Kelley, B. M., Kump, L. R., Lehrmann, D. J., et al.
(2016). Marine anoxia and delayed Earth system recovery after end-Permian extinction.
*Proceedings of the National Academy of Sciences*.
https://doi.org/10.1073/pnas.1515080113

Lemordant, L., Gentine, P., Swann, A. S., Cook, B. I., & Scheff, J. (2018). Critical impact of
vegetation physiology on the continental hydrologic cycle in response to increasing
$CO_2$. *Proceedings of the National Academy of Sciences*, *115*(16), 201720712.
https://doi.org/10.1073/pnas.1720712115

Lenton, T. M., & Britton, C. (2006). Enhanced carbonate and silicate weathering accelerates
recovery from fossil fuel $CO_2$ perturbations. *Global Biogeochemical Cycles*, *20*(3), 1–
12. https://doi.org/10.1029/2005GB002678

Li, L., Stewart, B., Zhi, W., Sadayappan, K., Ramesh, S., Kerins, D., et al. (2022). Climate
Controls on River Chemistry. *Earth's Future*, *10*(6), 1–17.
https://doi.org/10.1029/2021EF002603

Macdonald, F. A., Swanson-Hysell, N. L., Park, Y., Lisiecki, L., & Jagoutz, O. (2019). Arc-
continent collisions in the tropics set Earth's climate state. *Science*, *364*, 181–184.

Maher, K., & Chamberlain, C. P. (2014). Hydrologic regulation of chemical weathering and
the geologic carbon cycle. *Science*, *343*(6178), 1502–1504.
https://doi.org/10.1126/science.1250770

Mankin, J. S., Seager, R., Smerdon, J. E., Cook, B. I., & Williams, A. P. (2019). Mid-latitude
freshwater availability reduced by projected vegetation responses to climate change.
*Nature Geoscience*. https://doi.org/10.1038/s41561-019-0480-x

Milly, P. C. D., & Dunne, K. A. (2016). Potential evapotranspiration and continental drying.
*Nature Climate Change*, *6*, 946–949. https://doi.org/10.1038/NCLIMATE3046

Milly, P. C. D., & Dunne, K. A. (2020). Colorado River flow dwindles as warming-driven
loss of reflective snow energizes evaporation. *Science*, *9187*(February), eaay9187.
https://doi.org/10.1126/science.aay9187

Novick, K. A., Ficklin, D. L., Stoy, P. C., Williams, C. A., Bohrer, G., Oishi, A. C., et al.
(2016). The increasing importance of atmospheric demand for ecosystem water and
carbon fluxes. *Nature Climate Change*, *6*(11), 1023–1027.
https://doi.org/10.1038/nclimate3114

Otto-Bliesner, B. L. (1995). Continental drift, runoff, and weathering feedbacks: Implications
from climate model experiments. *Journal of Geophysical Research*, *100*(D6), 11537–

675  11548. https://doi.org/10.1029/95JD00591

Overpeck, J. T., & Udall, B. (2020). Climate change and the aridification of North America. *Proceedings of the National Academy of Sciences*, *0*, 202006323. https://doi.org/10.1073/pnas.2006323117

Panchuk, K., Ridgwell, A., & Kump, L. R. (2008). Sedimentary response to Paleocene-Eocene Thermal Maximum carbon release: A model-data comparison. *Geology*, *36*, 315–318. https://doi.org/10.1130/G24474A.1

Park, Y., Maffre, P., Godderis, Y., Macdonald, F. A., Anttila, E. S. C. C., Swanson-Hysell, N. L., et al. (2020). Emergence of the Southeast Asian islands as a driver for Neogene cooling. *Proceedings of the National Academy of Sciences*, *117*(41), 25319–25326. https://doi.org/10.1073/pnas.2011033117

Pendergrass, A. G., & Hartmann, D. L. (2014). The atmospheric energy constraint on global-mean precipitation change. *Journal of Climate*, *27*(2), 757–768. https://doi.org/10.1175/JCLI-D-13-00163.1

Penman, D. E. (2016). Silicate weathering and North Atlantic silica burial during the Paleocene-Eocene Thermal Maximum. *Geology*, (9). https://doi.org/10.1130/G37704.1

Penman, D. E., Turner, K. S., Sexton, P., Norris, R., Dickson, A. J., Boulila, S., et al. (2016). A carbonate compensation depth overshoot in the aftermath of the Paleocene-Eocene Thermal Maximum. *Nature Geoscience*. https://doi.org/10.1038/ngeo2757

Penman, D. E., Rugenstein, J. K. C., Ibarra, D. E., & Winnick, M. J. (2020). Silicate weathering as a feedback and forcing in Earth's climate and carbon cycle. *Earth-Science Reviews*, *209*, 103298. https://doi.org/10.1016/j.earscirev.2020.103298

Piao, S., Friedlingstein, P., Ciais, P., de Noblet-Ducoudre, N., Labat, D., & Zaehle, S. (2007). Changes in climate and land use have a larger direct impact than rising $CO_2$ on global river runoff trends. *Proceedings of the National Academy of Sciences*, *104*(39), 15242–15247. https://doi.org/10.1073/pnas.0707213104

Rugenstein, J. K. C., & Winkler, A. J. (2022). CH2O-CHOO v.1.1. Zenodo. https://doi.org/10.5281/zenodo.7219627.

van der Ploeg, R., Selby, D., Cramwinckel, M. J., Li, Y., Bohaty, S. M., Middelburg, J. J., & Sluijs, A. (2018). Middle Eocene greenhouse warming facilitated by diminished weathering feedback. *Nature Communications*, *9*(1), 2877. https://doi.org/10.1038/s41467-018-05104-9

Roderick, M. L., Greve, P., & Farquhar, G. D. (2015). On the assessment of aridity with changes in atmospheric $CO_2$. *Water Resources Research*, *51*(7), 5450–5463.

709       https://doi.org/10.1002/2015WR017031

710    Sagan, C., & Mullen, G. (1972). Earth and Mars: evolution of atmospheres and surface

711       temperatures. *Science*, *177*(4043), 52–56. https://doi.org/10.1126/science.177.4043.52

712    Scheff, J., & Frierson, D. M. W. (2014). Scaling potential evapotranspiration with

713       greenhouse warming. *Journal of Climate*, *27*(4), 1539–1558.

714       https://doi.org/10.1175/JCLI-D-13-00233.1

715    Scheff, J., Seager, R., Liu, H., & Coats, S. (2017). Are glacials dry? Consequences for

716       paleoclimatology and for greenhouse warming. *Journal of Climate*, *30*(17), 6593–6609.

717       https://doi.org/10.1175/JCLI-D-16-0854.1

718    Schlesinger, W. H., & Jasechko, S. (2014). Transpiration in the global water cycle.

719       *Agricultural and Forest Meteorology*, *189–190*, 115–117.

720       https://doi.org/10.1016/j.agrformet.2014.01.011

721    Shi, X., & Durran, D. R. (2014). The Response of Orographic Precipitation over Idealized

722       Midlatitude Mountains Due to Global Increases in $CO_2$. *Journal of Climate*, *27*(11),

723       3938–3956. https://doi.org/10.1175/JCLI-D-13-00460.1

724    Swann, A. L. S., Hoffman, F. M., Koven, C. D., & Randerson, J. T. (2016). Plant responses

725       to increasing $CO_2$ reduce estimates of climate impacts on drought severity. *Proceedings*

726       *of the National Academy of Sciences*, *113*(36), 10019–10024.

727       https://doi.org/10.1073/pnas.1604581113

728    Swanson-Hysell, N. L., & Macdonald, F. A. (2017). Tropical weathering of the Taconic

729       orogeny as a driver for Ordovician cooling. *Geology*, *45*(8), 719–722.

730       https://doi.org/10.1130/G38985.1

731    Them, T. R., Gill, B. C., Selby, D., Gröcke, D. R., Friedman, R. M., & Owens, J. D. (2017).

732       Evidence for rapid weathering response to climatic warming during the Toarcian

733       Oceanic Anoxic Event. *Scientific Reports*, *7*(1), 1–10. https://doi.org/10.1038/s41598-

734       017-05307-y

735    Torres, M. A., West, A. J., & Li, G. (2014). Sulphide oxidation and carbonate dissolution as a

736       source of $CO_2$ over geological timescales. *Nature*, *507*, 346–349.

737       https://doi.org/10.1038/nature13030

738    Uchikawa, J., & Zeebe, R. E. (2008). Influence of terrestrial weathering on ocean

739       acidification and the next glacial inception. *Geophys. Res. Lett.*, *35*(23).

740       https://doi.org/10.1029/2008GL035963

741    Ukkola, A. M., Prentice, I. C., Keenan, T. F., van Dijk, A. I. J. M., Viney, N. R., Myneni, R.

742       B., & Bi, J. (2016). Reduced streamflow in water-stressed climates consistent with $CO_2$

743    effects on vegetation. *Nature Climate Change*, 6, 75–78.

744    https://doi.org/10.1038/nclimate2831

745  Vervoort, P., Kirtland Turner, S., Rochholz, F., & Ridgwell, A. (2021). Earth System Model

746    Analysis of How Astronomical Forcing Is Imprinted Onto the Marine Geological

747    Record: The Role of the Inorganic (Carbonate) Carbon Cycle and Feedbacks.

748    *Paleoceanography and Paleoclimatology*, *36*(10), 1–20.

749    https://doi.org/10.1029/2020pa004090

750  Volk, T. (1987). Feedbacks between weathering and atmospheric $CO_2$ over the last 100

751    million years. *American Journal of Science*. https://doi.org/10.2475/ajs.287.8.763

752  Walker, J. C. G., Hays, P. B., & Kasting, J. F. (1981). A negative feedback mechanism for

753    the long-term stabilization of Earth's surface temperature. *Journal of Geophysical*

754    *Research*, *86*(C10), 9776–9782.

755  Wang-Erlandsson, L., van der Ent, R. J., Gordon, L. J., & Savenije, H. H. G. (2014).

756    Contrasting roles of interception and transpiration in the hydrological cycle – Part 1:

757    Temporal characteristics over land. *Earth System Dynamics*, *5*(2), 441–469.

758    https://doi.org/10.5194/esd-5-441-2014

759  Wei, Z., Yoshimura, K., Wang, L., Miralles, D. G., Jasechko, S., & Lee, X. (2017).

760    Revisiting the contribution of transpiration to global terrestrial evapotranspiration.

761    *Geophysical Research Letters*, *44*(6), 2792–2801.

762    https://doi.org/10.1002/2016GL072235

763  West, A. J. (2012). Thickness of the chemical weathering zone and implications for erosional

764    and climatic drivers of weathering and for carbon-cycle feedbacks. *Geology*, *40*(9), 811–

765    814. https://doi.org/10.1130/G33041.1

766  White, A. F., & Blum, A. E. (1995). Effects of climate on chemical weathering in

767    watersheds. *Geochimica et Cosmochimica Acta*, *59*(9), 1729–1747.

768    https://doi.org/10.1016/0016-7037(95)00078-E

769  Winkler, A. J., Myneni, R. B., Hannart, A., Sitch, S., Haverd, V., Lombardozzi, D., et al.

770    (2021). Slowdown of the greening trend in natural vegetation with further rise in

771    atmospheric $CO_2$. *Biogeosciences*, *18*(17), 4985–5010. https://doi.org/10.5194/bg-18-

772    4985-2021

773  Winnick, M., & Maher, K. (2018). Relationships between $CO_2$, thermodynamic limits on

774    silicate weathering, and the strength of the silicate weathering feedback. *Earth and*

775    *Planetary Science Letters*, *485*, 111–120.

776    https://doi.org/https://doi.org/10.1016/j.epsl.2018.01.005

777  Zeebe, R. E., & Caldeira, K. (2008). Close mass balance of long-term carbon fluxes from ice-
778      core $CO_2$ and ocean chemistry records. *Nature Geoscience*, *1*(5), 312–315.
779      https://doi.org/10.1038/ngeo185

780  Zeebe, R. E., & Lourens, L. J. (2019). Solar System chaos and the Paleocene–Eocene
781      boundary age constrained by geology and astronomy. *Science*, *365*, 926–929.

782  Zhang, X., Tang, Q., Zhang, X., & Lettenmaier, D. P. (2014). Runoff sensitivity to global
783      mean temperature change in the CMIP5 Models. *Geophysical Research Letters*, *41*,
784      5492–5498. https://doi.org/10.1002/2014GL061184.Received

785  Zhu, Z., Piao, S., Myneni, R. B., Huang, M., Zeng, Z., Canadell, J. G., et al. (2016). Greening
786      of the Earth and its drivers. *Nature Climate Change*, *6*, 791–795.
787      https://doi.org/10.1038/NCLIMATE3004

788

789  **Supporting Information References**

790  Arora, V.K., Boer, G.J., Friedlingstein, P., Eby, M., Jones, C.D., Christian, J.R., Bonan, G.,
791      Bopp, L., Brovkin, V., Cadule, P., Hajima, T., Ilyina, T., Lindsay, K., Tjiputra, J.F., Wu,
792      T., 2013. Carbon-concentration and carbon-climate feedbacks in CMIP5 earth system
793      models. J. Clim. 26, 5289–5314. https://doi.org/10.1175/JCLI-D-12-00494.1

794  Arora, V.K., Katavouta, A., Williams, R.G., Jones, C.D., Brovkin, V., Friedlingstein, P.,
795      Schwinger, J., Bopp, L., Boucher, O., Cadule, P., Chamberlain, M.A., Christian, J.R.,
796      Delire, C., Fisher, R.A., Hajima, T., Ilyina, T., Joetzjer, E., Kawamiya, M., Koven, C.D.,
797      Krasting, J.P., Law, R.M., Lawrence, D.M., Lenton, A., Lindsay, K., Pongratz, J.,
798      Raddatz, T., Séférian, R., Tachiiri, K., Tjiputra, J.F., Wiltshire, A., Wu, T., Ziehn, T.,
799      2020. Carbon – concentration and carbon – climate feedbacks in CMIP6 models and
800      their comparison to CMIP5 models. Biogeosciences 17, 4173–4222.

801  Berner, R.A., 2006. GEOCARBSULF: A combined model for Phanerozoic atmospheric O2
802      and CO2. Geochim. Cosmochim. Acta 70, 5653–5664.
803      https://doi.org/10.1016/j.gca.2005.11.032

804  Brady, P. V., 1991. The effect of silicate weathering on global temperature and atmospheric
805      CO2. J. Geophys. Res. 96. https://doi.org/10.1029/91jb01898

806  Brook, G., Folkoff, M., Box, E., 1983. A World Model of Soil Carbon Dioxide. Earth Surf.
807      Process. Landforms 8, 79–88.

808  Caves Rugenstein, J.K., Ibarra, D.E., von Blanckenburg, F., 2019. Neogene cooling driven by
809      land surface reactivity rather than increased weathering fluxes. Nature 571, 99–102.
810      https://doi.org/10.1038/s41586-019-1332-y

811    Gaillardet, J., Dupré, B., Louvat, P., Allegre, C., 1999. Global silicate weathering and CO2
812        consumption rates deduced from the chemistry of large rivers. Chem. Geol. 159, 3–30.

813    Graham, R.J., Pierrehumbert, R.T., 2020. Thermodynamic and Energetic Limits on
814        Continental Silicate Weathering Strongly Impact the Climate and Habitability of Wet,
815        Rocky Worlds.

816    Knutti, R., Rugenstein, M.A.A., Hegerl, G.C., 2017. Beyond equilibrium climate sensitivity.
817        Nat. Geosci. 10, 727–736. https://doi.org/10.1038/ngeo3017

818    Kump, L.R., Brantley, S.L., Arthur, M.A., 2000. Chemical weathering, atmospheric CO2,
819        and climate. Annu. Rev. Earth Planet. Sci. 28, 611–667.

820    Larsen, I.J., Montgomery, D.R., Greenberg, H.M., 2014. The contribution of mountains to
821        global denudation. Geology 42, 527–530. https://doi.org/10.1130/G35136.1

822    Lenton, T.M., Daines, S.J., Mills, B.J.W., 2018. COPSE reloaded: An improved model of
823        biogeochemical cycling over Phanerozoic time. Earth-Science Rev. 178, 1–28.
824        https://doi.org/10.1016/j.earscirev.2017.12.004

825    Maher, K., Chamberlain, C.P., 2014. Hydrologic regulation of chemical weathering and the
826        geologic carbon cycle. Science (80-. ). 343, 1502–1504.
827        https://doi.org/10.1126/science.1250770

828    Manabe, S., Wetherald, R.T., Milly, P.C.D., Delworth, T.L., Stouffer, R.J., 2004. Century-
829        scale change in water availability: CO2-quadrupling experiment. Clim. Change 64, 59–
830        76.

831    Milliman, J.D., Droxler, A.W., 1996. Neritic and pelagic carbonate sedimentation in the
832        marine environment: ignorance is not bliss. Geol. Rundschau 85, 496–504.

833    Moon, S., Chamberlain, C.P., Hilley, G.E., 2014. New estimates of silicate weathering rates
834        and their uncertainties in global rivers. Geochim. Cosmochim. Acta 134, 257–274.
835        https://doi.org/10.1016/j.gca.2014.02.033

836    Myhre, G., Highwood, E.J., Shine, K.P., Stordal, F., 1998. New estimates of radiative forcing
837        due to well mixed greenhouse gases. Geophys. Res. Lett. 25, 2715–2718.

838    Prentice, I.C., Harrison, S.P., 2009. Ecosystem effects of CO2 concentration: Evidence from
839        past climates. Clim. Past 5, 297–307. https://doi.org/10.5194/cp-5-297-2009

840    Scheff, J., Seager, R., Liu, H., Coats, S., 2017. Are glacials dry? Consequences for
841        paleoclimatology and for greenhouse warming. J. Clim. 30, 6593–6609.
842        https://doi.org/10.1175/JCLI-D-16-0854.1

843    Shields, G.A., Mills, B.J.W., 2017. Tectonic controls on the long-term carbon isotope mass
844        balance. Proc. Natl. Acad. Sci. 114, 4318–4323.

845     https://doi.org/10.1073/pnas.1614506114

846  Volk, T., 1987. Feedbacks between weathering and atmospheric CO2 over the last 100

847     million years. Am. J. Sci. https://doi.org/10.2475/ajs.287.8.763

848  Wallmann, K., 2001. Controls on the Cretaceous and Cenozoic evolution of seawater

849     composition, atmospheric CO2 and climate. Geochim. Cosmochim. Acta 65, 3005–

850     3025. https://doi.org/10.1016/S0016-7037(01)00638-X

851  West, A.J., 2012. Thickness of the chemical weathering zone and implications for erosional

852     and climatic drivers of weathering and for carbon-cycle feedbacks. Geology 40, 811–

853     814. https://doi.org/10.1130/G33041.1

854  Winnick, M., Maher, K., 2018. Relationships between CO2, thermodynamic limits on silicate

855     weathering, and the strength of the silicate weathering feedback. Earth Planet. Sci. Lett.

856     485, 111–120. https://doi.org/https://doi.org/10.1016/j.epsl.2018.01.005

857  Zhang, Xuejun, Tang, Q., Zhang, Xuezhen, Lettenmaier, D.P., 2014. Runoff sensitivity to

858     global mean temperature change in the CMIP5 Models. Geophys. Res. Lett. 41, 5492–

859     5498. https://doi.org/10.1002/2014GL061184.Received

860

861

862

863

**Geologic carbon cycle constraints on the terrestrial hydrological response to higher atmospheric CO₂**

Jeremy K. C. Rugenstein[1,2] and Alexander J. Winkler[2,3]

[1]Department of Geosciences, Colorado State University, Fort Collins, CO, USA
[2]Max Planck Institute for Meteorology, Hamburg, Germany
[3]Max Planck Institute for Biogeochemistry, Jena, Germany

**Contents of this file**

**Introduction**

This supplementary file contains a detailed description of the model equations used in CH2O-CHOO and their derivation. It also contains several figures relevant to understanding the arguments in the main text as well as tables that contain model parameters, both for CH2O-CHOO and for the Earth system models that were investigated for their runoff sensitivity.

**Text S1. Model Framework**

We modify a carbon cycle model to incorporate runoff ($q$) into the equations that predict carbon mass balance. CH2O-CHOO is adapted from and is a simplified version of CLiBeSO-W (Caves Rugenstein et al., 2019), which is itself based upon aspects of the COPSE and GEOCARB models (Berner, 2006; Lenton et al., 2018; Shields and Mills, 2017). The mass balance forward model solves for the time-varying reservoirs of carbon ($C$) and alkalinity ($A$) as a function of the major fluxes of $C$ and $A$ to and from the ocean-atmosphere, according to equations 1 and 2:

$$\frac{dC}{dt} = F_{carbw} + F_{orgw} + F_{volc} - F_{carbb} - F_{orgb} \tag{1},$$
and

$$\frac{dA}{dt} = 2F_{carbw} + 2F_{silw} - 2F_{carbb} \qquad (2),$$

where $F_{carbw}$, $F_{orgw}$, and $F_{silw}$ are the carbonate, organic, and silicate weathering fluxes, $F_{volc}$ is the volcanic flux, and $F_{carbb}$ and $F_{orgb}$ are the carbonate and organic burial fluxes [mol C/yr].

We treat $F_{silw}$ as a function of $q$ and the concentration of silicate-weathering derived bicarbonate ($[C]_{sil}$):

$$F_{silw} = F_{silw,0} \times R_q \times R_{[c]} \qquad (3),$$

where $F_{silw,0}$ is the initial, pre-perturbation weathering flux, $R_q$ is the ratio of $q$ at time $t$ to initial $q$ ($q_0$), and $R_{[c]}$ is the ratio of $[C]_{sil}$ at time $t$ to the initial $[C]_{sil}$ ($[C]_{sil,0}$). We calculate $q$ as an exponential function of global temperature ($T$ [K]), which is itself logarithmically related to atmospheric $CO_2$ (Knutti et al., 2017; Myhre et al., 1998):

$$q = q_0(1 + \lambda_q)^{\Delta T} \qquad (4),$$

where $\lambda_q$ describes the sensitivity of $q$ to $T$ [%/K] (*i.e.*, the $q$-sensitivity), and $\Delta T$ is calculated via its relationship to climate sensitivity:

$$\Delta T = S_{eq} log_2(R_{CO2}) \qquad (5),$$

where $S_{eq}$ is the equilibrium climate sensitivity and $R_{CO2}$ is the ratio of atmospheric $CO_2$ at time $t$ ($CO_{2,t}$) and the pre-perturbation $CO_2$ ($CO_{2,0}$).

The value of $[C]_{sil}$ is calculated using modified equations from Maher and Chamberlain (2014) (*i.e.*, the MAC model, following derivations in Graham and Pierrehumbert (2020)). These equations permit us to explicitly incorporate the effect of $T$, $q$, and weathering zone $pCO_2$—all sensitive to atmospheric $CO_2$ and climate—on $[C]_{sil}$.

$$[C]_{sil} = [C]_{sil,eq} \left( \frac{\frac{Dw}{q}}{1 + \frac{Dw}{q}} \right) \qquad (6),$$

where $[C]_{sil,eq}$ is the maximum, equilibrium concentration of silicate-derived bicarbonate and $Dw$ is the Damköhler weathering coefficient, which is a term that encapsulates the reactivity of the weathering zone and time required to reach equilibrium. Following Maher and Chamberlain (2014), we define $Dw$ as:

$$Dw = \frac{L_\phi r_{max} \frac{1}{1 + Ts \times r_{eff}}}{[C]_{sil,eq}} \qquad (7),$$

where $L_\phi$ is the reactive length scale (held constant for our simulations), $r_{max}$ is the theoretical maximum reaction rate (held constant for our simulations), $Ts$ is the age of the weathering zone and is a key variable describing the reactivity of the weathering zone, and $r_{eff}$ is the effective reaction rate. This effective reaction rate is defined as:

$$r_{eff} = ke^{\left[\left(\frac{Ea}{Rg}\right)\left(\frac{1}{T} - \frac{1}{T_0}\right)\right]}$$ (8),

where $R_g$ is the universal gas constant [J/K/mol], $Ea$ is the activation energy [J/mol], and the exponential term is an Arrhenius function to describe the effect of $T$ on reaction rates (Brady, 1991; Kump et al., 2000). The coefficient $k$ [y$^{-1}$] encapsulates the effects of mineral surface area, molar mass, and the reference reaction rate (all assumed constant) that modulate the effect of $T$ on $r_{eff}$.

Lastly, [C]$_{sil,eq}$ is modified by the availability of reactant, which here is assumed to be dominantly $CO_2$. We calculate this effect as a function of weathering zone $pCO_2$ assuming open-system $CO_2$ dynamics, following Winnick and Maher (2018):

$$[C]_{sil,eq} = [C]_{sil,eq,0}\left(R_{CO2,wz}\right)^{0.316}$$ (9),

where [C]$_{sil,eq,0}$ is the pre-perturbation, initial value of [C]$_{sil,eq}$. $R_{CO2,wz}$ is the ratio of weathering zone $pCO_2$ at time $t$ ($WZ_{CO2}$) to the initial weathering zone $pCO_2$ pre-perturbation ($WZ_{CO2,0}$). We calculate $R_{CO2,wz}$ using a formulation proposed by Volk (1987) that links weathering zone $pCO_2$ with the primary source of that $CO_2$, which is aboveground terrestrial gross primary productivity (GPP). Here, $WZ_{CO2}$ is calculated using an equation that links GPP, $CO_2$ fertilization on GPP, and weathering zone $CO_2$:

$$WZ_{CO2} = \left[R_{GPP}\left(1 - \frac{CO_{2,0}}{WZ_{CO2,0}}\right) + \frac{CO_2}{WZ_{CO2,0}}\right]WZ_{CO2,0} + \left(CO_2 - CO_{2,0}\right)$$ (10).

Here, $R_{GPP}$ is the ratio of GPP at time $t$ to the pre-perturbation GPP ($GPP_o$) and the last term on the right-hand side of the equation ensures that $WZ_{CO2}$ is always greater than atmospheric $CO_2$. GPP is calculated using a Michaelis-Menton formulation, following Volk (1987):

$$GPP = GPP_{max}\left[\frac{CO_2 - CO_{2,min}}{CO_{2,half} + \left(CO_2 - CO_{2,min}\right)}\right]$$ (11),

where $GPP_{max}$ is the maximum possible global terrestrial GPP, $CO_{2,min}$ is the $CO_2$ at which photosynthesis is balanced exactly by photorespiration, and $CO_{2,half}$ is the $CO_2$ at which GPP is equivalent to 50% $GPP_{max}$:

$$CO_{2,half} = \left(\frac{GPP_{max}}{GPP_0} - 1\right)\left(CO_{2,0} - CO_{2,min}\right)$$ (12).

We choose a $CO_{2,min}$ of 100 ppm based upon evidence for widespread $CO_2$ starvation at the Last Glacial Maximum (LGM) (Prentice and Harrison, 2009; Scheff et al., 2017), which had an atmospheric $CO_2$ of ~180 ppm. We also assume that $GPP_{max}$ is equal to twice $GPP_0$, though our results are insensitive to this parameter. Lastly, we assume that $WZ_{CO2,0}$ is 10x larger than $pCO_{2,0}$ given evidence that soil $CO_2$ is typically elevated above atmospheric levels by approximately an order of magnitude (Brook et al., 1983).

**Figure S1.** The percentage change in $[C]_{sil}$ as atmospheric $CO_2$ doubles as a function of the $q$-sensitivity, using the Maher and Chamberlain (2014) formulation of weathering. Generally, $[C]_{sil}$ increases even if $q$ increases, unless $q$ increases are so large (8-16 %/K) that increasing $q$ causes dilution that overwhelms the effect from rising temperatures and increasing soil $pCO_2$. However, changes in $[C]_{sil}$ are less than 1:1 with changes in $q$, as indicated by the lower slope of the black lines relative to the 1:1 line (red). Solid line uses the standard parameters (Table S1); dashed line assumes an 8° K/$CO_2$ doubling equilibrium climate sensitivity; dot-dashed line assumes that soil $pCO_2$ scales 1:1 with atmospheric $pCO_2$ (rather than using the Volk (1987) formulation that relates soil $pCO_2$ to atmospheric $pCO_2$); long dashed line uses a higher activation energy ($Ea = 76$ kJ/mol).
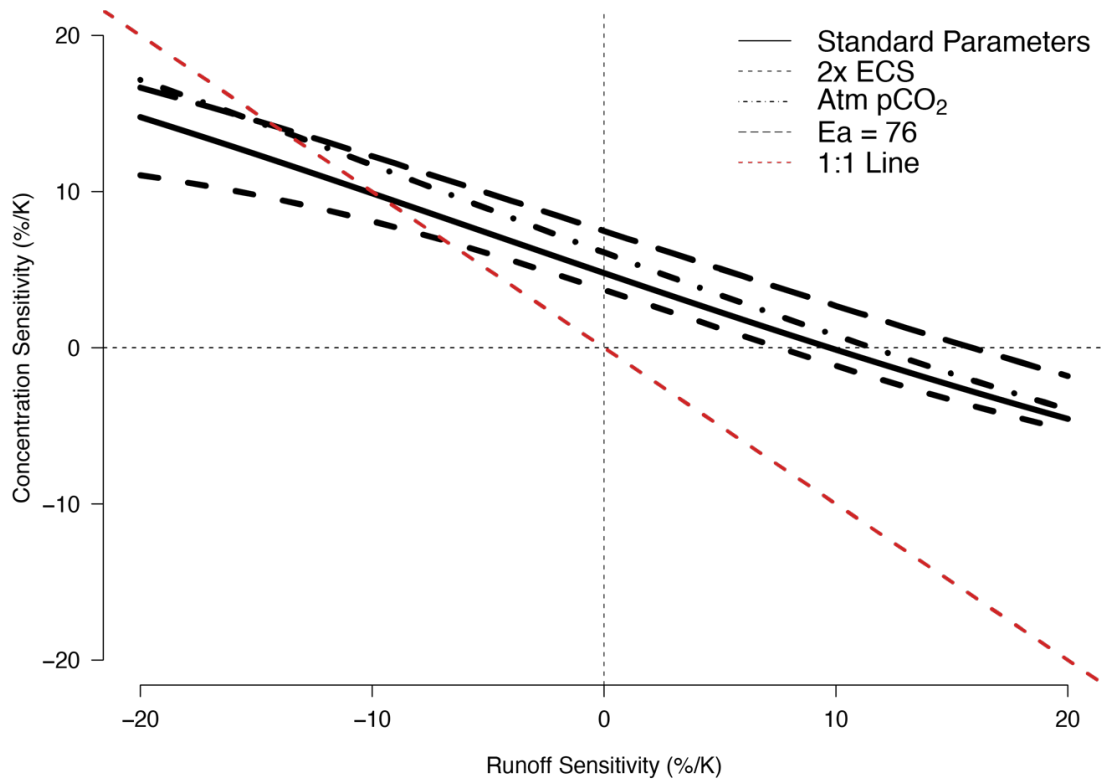
**Figure S2.** Effect of variations of weathering zone age ($T_s$) on the recovery time using the West (2012) formulation of weathering zone fluxes. Red line uses the standard values (Table S1) and the Maher and Chamberlain (2014) formulation of weathering fluxes. Gray vertical bar indicates the range of runoff sensitivity estimated using the C4MIP model ensemble (see main text).
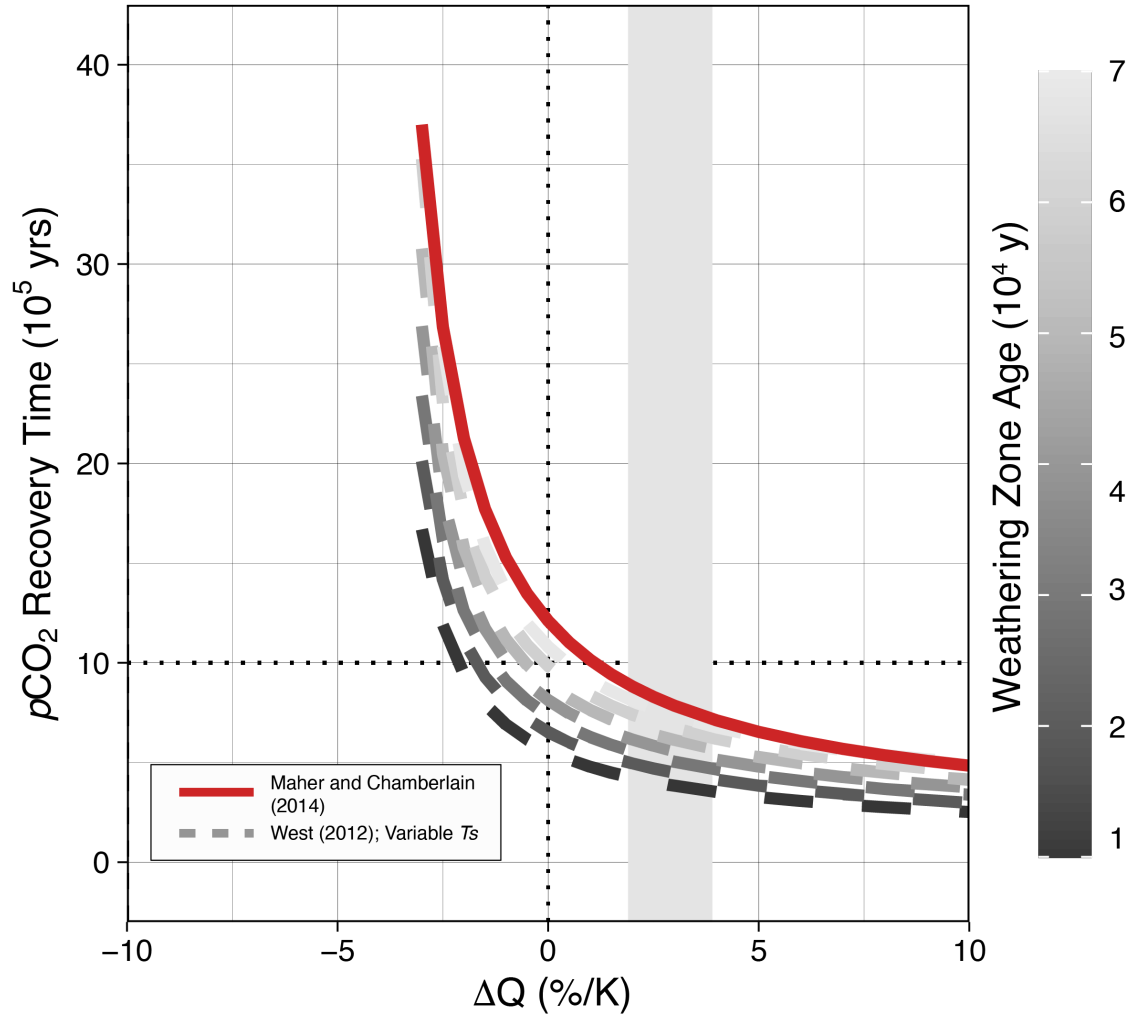
**Table S1**. Parameters used in the CH2O-CHOO model, organized by model sub-component. Sources are listed if different from the original model formulation in Maher and Chamberlain (2014) or West (2012).

| Parameters | Optimized Values | Units | Source |
|---|---|---|---|
| | Climate parameters | | |
| Earth System Sensitivity | 4 | K/$CO_2$ doubling | Knutti et al. (2017) |
| Initial Earth Surface $T$ | 15 | K | |
| $q_0$ | 0.3 | m/yr | Manabe et al. (2004) |
| $pCO_2$ | 400 | ppm | |
| pH | 8.15 | – | |
| | Carbon cycle model parameters | | |
| $F_{silw,0}$ | 6 | $10^{12}$ mol C/yr | Moon et al. (2014) |
| $F_{carbw,0}$ | 12 | $10^{12}$ mol C/yr | Gaillardet et al. (1999) |
| $F_{orgw,0}$ | 6 | $10^{12}$ mol C/yr | Berner (2006) |
| $F_{carbb,0}$ | 18 | $10^{12}$ mol C/yr | Milliman and Droxler (1996) |
| $F_{orgb,0}$ | 6 | $10^{12}$ mol C/yr | |
| $F_{volc,0}$ | 6 | $10^{12}$ mol C/yr | Wallmann (2001) |
| | Maher and Chamberlain (2014) model parameters | | |
| $r_{eff}$ | 8.7 | $10^{-6}$ mol/m²/yr | |
| $m$ | 270 | g/mol | |
| $A$ | 0.1 | m²/g | |
| $r_{max}$ | 1085 | $\mu$mol/L/yr | |
| $L_\phi$ | 0.1 | m | |
| $Ts$ | 2 | $10^4$ yr | Larsen et al. (2014) |
| $C_{eq}$ | 374 | $\mu$mol/L | |
| $Ea$ | 38 | kJ/mol | |
| | West (2012) model parameters | | |
| $K$ | 2.6 | $10^{-4}$ | |
| $K_w$ | 7.6 | $10^{-5}$ | |
| $z$ | 8.9 | – | |
| $X_m$ | 0.09 | – | |
| $\sigma$ | 0.89 | – | |

**Table S2**. Overview of CMIP5/6 models included in this study (Arora et al., 2020, 2013)

| Models | MPI-ESM1-2-LR | UKESM1-0-LL | CNRM-ESM2-1 | IPSL-CM6A-LR | ACCESS-ESM1-5 | NorESM1-ME | CESM1-BGC | IPSL-CM5A-LR |
|---|---|---|---|---|---|---|---|---|
| Generation | CMIP6 | CMIP6 | CMIP6 | CMIP6 | CMIP6 | CMIP5 | CMIP5 | CMIP5 |
| No. of PFTs | 13 | 13 | 16 | 15 | 13 | 16 | 16 | 5 |
| Land Model | JSBACH3.2 | JULES-ES-1.0 | ISBA-CTRIP | ORCHIDEE, branch 2.0 | CABLE2.4 with CASA-CNP | CLM4 | CLM4 | ORCHIDEE |
| Land resolution | 1.8° ×1.8° | 1.875° × 1.25° | 1.4° × 1.4° | 2.5° × 1.3° | 1.875° × 1.25° | 2.5° × 1.9° | 0.9° × 1.2° | 2° × 0.5°—2° |
| Dynamic vegetation | Yes | Yes | No | No | No | No | No | No |
| Nitrogen cycle | Yes | Yes | No | No | Yes | Yes | Yes | No |
| Fire | Yes | No | Yes | No | No | Yes | Yes | Yes |